

1
2
3
4
5
6
7
8
9
10
11
12
13
14
15
16
17
18
19
20
21
22
23
24

**Multidecadal Ocean Temperature and Salinity Variability in the Tropical North Atlantic:
Linking with the AMO, AMOC and Subtropical Cell**

Chunzai Wang ¹

Liping Zhang ^{2 & 1}

¹NOAA Atlantic Oceanographic and Meteorological Laboratory
Miami, Florida

²Cooperative Institute for Marine and Atmospheric Studies
University of Miami
Miami, Florida

Journal of Climate
February 2013

Corresponding author address: Dr. Liping Zhang, Physical Oceanography Division,
NOAA/Atlantic Oceanographic and Meteorological Laboratory, 4301 Rickenbacker Causeway,
Miami, FL 33149. E-mail: Liping.Zhang@noaa.gov.

Abstract

The Atlantic multidecadal oscillation (AMO) is characterized by the sea surface warming (cooling) of the entire North Atlantic during its warm (cold) phase. Both observations and most of CMIP5 models also show that the warm (cold) phase of the AMO is associated with a surface warming (cooling) and a subsurface cooling (warming) in the tropical North Atlantic (TNA) Ocean. It is further shown that the warm phase of the AMO corresponds to a strengthening of the Atlantic meridional overturning circulation (AMOC) and a weakening of the Atlantic subtropical cell (STC), both of which induce an anomalous northward current in the TNA subsurface ocean. Because the mean meridional temperature gradient of the subsurface ocean is positive due to the temperature dome around 9°N, the advection by the anomalous northward current cools the TNA subsurface ocean during the warm phase of the AMO. The opposite is true during the cold phase of the AMO. It is concluded that the anticorrelated ocean temperature variation in the TNA associated with the AMO is caused by the meridional current variation induced by variability of the AMOC and STC, but the AMOC plays a more important role than the STC. Observations do not seem to show an obvious anticorrelated salinity relation between the TNA surface and subsurface oceans, but most of CMIP5 models simulate an out-of-phase salinity variation. Similar to the temperature variation, the mechanism is the salinity advection by the meridional current variation induced by the AMOC and STC associated with the AMO.

1 **1. Introduction**

2 One of the most important climate variations in the Atlantic is the Atlantic multidecadal
3 oscillation (AMO) which is a basin-wide mode in the entire North Atlantic and is defined by the
4 North Atlantic sea surface temperature (SST) anomalies (e.g., Enfield et al. 2001; Knight et al.
5 2005). The AMO has significant regional and global climate associations, such as the
6 Northeast Brazilian and African Sahel rainfall (Folland et al. 1986; Rowell et al. 1995; Folland et
7 al. 2001; Rowell 2003; Wang et al. 2012), the Atlantic warm pool (Wang et al. 2008; Zhang et al.
8 2012a; Wang et al. 2013) and Atlantic hurricanes (Goldenberg et al. 2001; Wang and Lee 2009),
9 and North American and European summer climate (Enfield et al. 2001; McCabe et al. 2004;
10 Sutton and Hodson 2005). In spite of its importance, the mechanism of the AMO is still
11 unclear. One of the most popular arguments is that the AMO is induced by the Atlantic
12 meridional overturning circulation (AMOC) variations and associated heat transport fluctuations
13 (Folland et al. 1986; Gray et al. 1997; Delworth and Mann 2000; Knight et al. 2005). Some of
14 modeling studies indicate that the solar variability and/or volcanoes play a role in the AMO
15 (Hansen et al. 2005; Otterå et al. 2010), or the external forcing aerosols can be as a primary
16 driver for the AMO (Booth et al. 2012). A recent observational study shows that a positive
17 feedback between the SST and dust aerosol in the North Atlantic via Sahel rainfall variability
18 may be a mechanism for the AMO (Wang et al. 2012).

19 As a basin-wide SST mode in the North Atlantic, the AMO warming or cooling is also
20 manifested in the tropical North Atlantic (TNA) SST anomalies. That is, the TNA SST
21 variation on multidecadal timescales is in phase with the AMO. The variations of the TNA

1 SST and upper ocean temperature are very important because they directly affect hurricane
2 activity in the North Atlantic (e.g., Shay et al. 2000; Wang et al. 2008). Here, we focus on the
3 TNA ocean temperature variations associated with the AMO. Zhang (2007) and Wang et al.
4 (2010) showed that the TNA SST anomalies are inversely related to or anticorrelated with the
5 subsurface ocean temperature anomalies in association with the AMO. In other words, the
6 TNA SST anomalies vary out-of-phase with the subsurface ocean temperature anomalies on
7 multidecadal timescales. In a study for comparing several ocean reanalysis products by Corre
8 et al. (2012), the variation of the TNA subsurface temperature with the AMO can also be seen
9 (their Fig. 10). Zhang (2007) suggested that the anticorrelated change between the TNA
10 surface and subsurface temperatures is a distinctive signature of the AMOC variation based on
11 the coupled GFDL_CM2.1 model and thus can be taken as an AMOC fingerprint. The
12 mechanism of the anticorrelated change proposed by Zhang (2007) is associated with the
13 AMOC-induced TNA subsurface thermocline adjustment.

14 In the present paper, we further show that the anticorrelated multidecadal variation does
15 exist in observational data and climate models of the Coupled Model Intercomparison Project
16 phase 5 (CMIP5). Using observational data and CMIP5 models, we demonstrate that the TNA
17 subsurface cooling (warming) during the warm (cold) phase of the AMO is largely due to the
18 meridional advection by the anomalous northward (southward) current, whereas the subsurface
19 thermocline adjustment plays a secondary role. The present paper further shows that the
20 anomalous northward (southward) current is attributed to variability of the AMOC and the
21 shallow Atlantic subtropical cell (STC) (e.g., Malanotte-Rizzoli et al. 2000; Zhang et al. 2003).

1 In addition, the paper also discusses variability of the TNA surface and subsurface salinity on
2 multidecadal timescales.

3 The paper is organized as follows. Section 2 briefly introduces the data sets and methods
4 used in this paper. The assessment of the anticorrelated multidecadal variation between TNA
5 surface and subsurface temperatures in observational data and CMIP5 models is presented in
6 Section 3. The mechanisms of the anticorrelated multidecadal variation are analyzed and
7 examined in Section 4. Section 5 shows a linkage among the AMO, AMOC, STC, and the
8 TNA surface and subsurface ocean temperature variation. Section 6 briefly investigates the
9 multidecadal variation of salinity in the TNA Ocean. The paper is concluded with a summary
10 and discussion in Section 7.

11

12 **2. Data sets and methods**

13 Several data sets are used in this study. The first one is the improved extended
14 reconstructed SST (ERSST), with a 2° latitude by 2° longitude resolution (Smith and
15 Reynolds 2004). The second data set is the Simple Ocean Data Assimilation (SODA)
16 (Carton and Giese 2008). The SODA uses an ocean general circulation model (GCM) to
17 assimilate available temperature and salinity observations. The product is a gridded data set
18 of oceanic variables with monthly values at a $0.5^\circ \times 0.5^\circ$ latitude-longitude horizontal
19 resolution and 40 vertical levels (The SODA product is sometimes called observational data).
20 The ocean model surface boundary conditions are taken from a new atmospheric data set
21 designated as 20CRv2 (20th Century Reanalysis version 2), which contains the

1 synoptic-observation-based estimate of global tropospheric variability spanning 1871 to 2008
2 at 6-hourly temporal and 2° spatial resolutions (Compo et al. 2011). The version 2.2.4 of the
3 SODA data is used, with the time covering from 1871 to 2008. Additionally, the objectively
4 analyzed temperature and salinity version 6.7 (Ishii et al. 2006) at 24 levels in the upper ocean
5 of 1500 m from 1945-2010 is also used. The analysis is based on the World Ocean Database,
6 the global temperature-salinity in the tropical Pacific from IRD/France, and the Centennial in
7 situ Observation Based Estimates (COBE) SST. The Ishii et al. analysis also includes the
8 Argo profiling buoy data in the final several years and the XBT depth bias correction.

9 Eighteen coupled GCM output data sets of the “historical” simulations provided to the
10 Intergovernmental Panel on Climate Change Fifth Assessment Report (IPCC-AR5) are also used
11 in this study. The modeling center and country, IPCC model name, and temporal coverage are
12 shown in Table 1. The model data can be downloaded from the website of the Coupled Model
13 Intercomparison Project phase 5 (CMIP5; Taylor et al. 2012) (<http://cmip-pcmdi.llnl.gov/cmip5/>).
14 The historical runs are forced by observed atmospheric composition changes which reflect both
15 anthropogenic (greenhouse gases) and natural sources (volcanic influences, solar forcing,
16 aerosols and emissions of short-lived species and their precursors) and, for the first time,
17 including time-evolving land cover. The historical runs cover much of the industrial period
18 from the mid-nineteenth century to the present and are sometimes referred to as “twentieth
19 century” simulations. All of the coupled GCMs are coupled freely without flux correction.
20 Variables of surface heat flux, wind, temperature, salinity, and current are used in this study.

21 Several statistical methods are used in this study, such as the lead-lag correlation and linear

1 regression. To demonstrate possible mechanisms of the surface and subsurface ocean
2 temperature variations in the TNA, we conduct the heat budget analysis of the zonal mean
3 temperature. The ocean heat budget analysis is based on the temperature equation in which the
4 local temperature change depends on ocean temperature advection terms and surface heat flux.
5 Our major purpose is to qualitatively rather than quantitatively assess the relative importance of
6 the surface heat flux and ocean advections in generating the low-frequency temperature variation.
7 Since we focus on the zonal mean surface and subsurface temperature anomalies, the ocean
8 advection in the zonal direction can be neglected. All the data are linearly detrended and
9 smoothed by a 7-year low-frequency filter (we use the fifth order Butterworth low-pass filter).

10

11 **3. Anticorrelated variation of TNA surface and subsurface ocean temperatures**

12 *a. Observed results*

13 We first use the SODA and Ishii data to calculate the AMO indices (Figs. 1a, e) on
14 low-frequency (or multidecadal) timescales. We then regress the Atlantic zonal mean ocean
15 temperatures onto the multidecadal AMO indices (Figs. 1b, f). Consistent with the previous
16 studies of Zhang (2007) and Wang et al. (2010), the TNA Ocean shows an anticorrelated
17 variation between the surface and subsurface temperatures on multidecadal timescales. It can
18 be seen that the surface temperature is characterized by a basin-wide and uniform warming
19 (cooling) in the entire North Atlantic with a maximum magnitude occurring in the subpolar
20 region during the warm (cold) phase of the AMO, in agreement with the definition of the AMO
21 index. The penetration depth of the surface warming is latitude-dependent. The higher the

1 latitude is, the deeper the surface warming penetrates. On the contrary, the TNA subsurface
2 ocean temperature tends to become cool (warm) during the warm (cold) phase of the AMO. In
3 the TNA Ocean, the anomalous cooling appears below 100 m and penetrates down to 1500 m,
4 with a maximum cooling around 200 m between 8°N and 20°N. North of 20°N, the location of
5 cooling anomaly becomes deeper.

6 The anticorrelated surface and subsurface temperature variation or vertical dipole
7 temperature structure in the TNA occurs only on multidecadal timescales. The low panels of
8 Fig. 1 show the regressions of the TNA ocean temperature anomalies at each depth onto the
9 TNA SST anomalies (averaged in the region of 8°N-20°N and coast to coast) on interannual and
10 multidecadal timescales from the SODA and Ishii data. It is shown that the dipole structure in
11 the TNA appears only on multidecadal timescales, whereas on interannual timescales the
12 temperature profile exhibits a uniform positive regression between the surface and subsurface
13 oceans. This suggests that the TNA dipole temperature anomaly should originate from the
14 relatively slow ocean adjustment, particularly in the high latitude where the ocean has a long
15 time memory.

16 To further demonstrate the anticorrelated variation, we plot the multidecadal time series of
17 temperature anomalies at the sea surface and 200 m, and vertically averaged temperature
18 anomalies from 0-400 m using the SODA and Ishii data (Fig. 2). Since the Ishii data are
19 available only from the middle of the 20th century, for the purpose of consistency we plot both
20 the time series starting from 1945. The anticorrelated or out-of-phase relationship between the
21 SST anomalies and temperature anomalies at 200 m is obvious in both the data sets, with the

1 correlation coefficients of -0.95 and -0.93 in the SODA and Ishii data, respectively. When the
2 TNA surface ocean is warm (cold), the subsurface temperature at 200 m is cold (warm). Since
3 the subsurface variation is deeper and larger than the surface (Figs. 1b, f), the vertically averaged
4 temperature anomalies between 0-400 m mainly follow the subsurface temperature anomalies
5 such as those at 200 m.

6

7 *b. CMIP5 simulations*

8 The AMO indices from 18 CMIP5 model simulations and the ERSST observation are
9 shown in Fig. 3. CMIP5 models show a significant decadal to multidecadal variation of the
10 AMO; however, they strongly disagree both in phase and strength with the observation. To
11 some degree, CMIP5 simulations share a relatively better resemblance with the observation than
12 CMIP3 models (Medhaug and Furevik 2011), particularly in the last two decades. The two
13 main discrepancies between the model and observation are during the early 20th century
14 (1900-1920) when the models underestimate the cooling, and during the subsequent mid-century
15 warming (1925-1965) when the models are generally too cool. This could be due to errors in
16 the observations, inadequacy in the modeled response to external forcing or forcing that is not
17 included in model simulations, or due to different internal variations in different models. The
18 contributions of external forcing and internal variation to the North Atlantic SST in climate
19 models are recently in debate (e.g., Ting et al. 2009; Booth et al. 2012; Terray 2012; Zhang et al.
20 2013). It is possible that a combination of both effects is attributed to the 20th century
21 multidecadal SST variation in the North Atlantic; however, their relative importance remains an

1 issue to be determined.

2 The regression of the Atlantic zonal mean temperatures onto the AMO index for individual
3 models is shown in Fig. 4. Of 18 CMIP5 models, 12 models are able to simulate the
4 anticorrelated variation between the TNA surface and subsurface ocean temperatures:
5 bcc-csm1-1, CanESM2, CNRM-CM5, CSIRO-MK3-6-0, GFDL-ESM2G, GFDL-ESM2M,
6 GISS-E2-R, HadGEM2-ES, MIROC5, MIROC-ESM-CHEM, MPI-ESM-P and MRI-CGCM3
7 (Figs. 4a-l). These models simulate a surface warming (cooling) anomaly in the TNA Ocean
8 and a subsurface cooling (warming) anomaly with the maximum around 200 m between
9 8°N-20°N during the warm (cold) phase of the AMO. The other 6 models do not well simulate
10 the TNA subsurface cooling during the warm phase of the AMO: FGOALS-g2, GISS-E2-H,
11 IPSL-CM5A-LR, IPSL-CM5A-MR, MIROC-ESM, and CCSM4 (Figs. 1m-r). In the following
12 section, we will examine physical mechanisms that are responsible for the vertical temperature
13 dipole structure associated with the AMO.

14

15 **4. Mechanisms of surface and subsurface ocean temperature variations**

16 *a. Long-term mean states*

17 To help the understanding of the ocean temperature variations in the TNA, we first present
18 the oceanic and atmospheric mean states in the TNA. Long-term mean surface net heat flux in
19 the TNA is characterized by a heat loss from the ocean in the west and a heat gain in the east
20 (Fig. 5a). The former is due to the strong trade wind-induced turbulent heat flux, whereas the
21 latter is largely associated with the radiative heat flux. Surface freshwater flux (evaporation

1 minus precipitation) exhibits a freshwater gain in the Intertropical Convergence Zone (ITCZ)
2 region (Fig. 5b) where the surface wind convergence is accompanied with the ascending motion.
3 In the north of the ITCZ, the TNA is covered by a freshwater loss as a result of the surface wind
4 divergence and the descending motion. Fig. 5c displays the vertical structure of the zonal mean
5 ocean temperature in the TNA region. In the surface, the temperature gradually decreases with
6 the latitude, resulting from the solar radiation. Thus, the mean meridional SST gradient is
7 negative near the surface, except near the equator because of the equatorial upwelling (Fig. 6a).
8 In the subsurface, it is interesting to see that there is a temperature dome at 9°N where the ITCZ
9 is located and the isotherms on both sides tend to tilt upward (Fig. 5c). On the equatorward side
10 of the temperature dome, the mean meridional temperature gradient in the subsurface ocean is
11 negative, while the opposite is true on the poleward side (Fig. 6a). Similar to the temperature
12 structure, the zonal mean salinity is also represented by a salinity dome at 9°N (Fig. 5d).
13 Therefore, the mean meridional salinity gradient also features a dipole pattern across 9°N (Fig.
14 6b). In the surface, salinity is low in the ITCZ region and high in the subtropics (Fig. 5d) and
15 thus gives rise to a positive meridional salinity gradient north of the dome (Fig. 6b), which can
16 be expected from the surface net freshwater flux (Fig. 5b). Further inspection finds that the
17 maximum positive meridional temperature and salinity gradients in the subsurface locate in the
18 depth of about 200 m between 8-16°N (Figs. 6a, b), which collocates with the maximum
19 multidecadal subsurface TNA temperature variation (Fig. 1).

20 The vertical temperature gradient is always positive in the TNA with the maximum gradient
21 in the upper layer from the equator to 15°N (Fig. 6c). Contrary to the temperature, there is a

1 dipole structure in the vertical salinity gradient, with a negative gradient in the upper 100 m and
2 a positive salinity gradient below (Fig. 6d). The surface negative salinity gradient can be
3 attributed to the surface freshwater gain and the intrusion of subtropical high salinity in the
4 subsurface (Fig. 5b). As expected, the zonal mean meridional ocean velocity displays a
5 northward current above the Ekman layer, which results from the trade wind-induced northward
6 Ekman drift (Fig. 5e). On the contrary, water tends to flow southward in the interior that can be
7 explained by the Sverdrup relation. The zonal mean vertical ocean velocity in the TNA is
8 generally characterized by an upwelling south of 14°N and a downwelling in the north (Fig. 5f),
9 which is primarily due to the Ekman transport-induced vertical motion.

10

11 *b. Physical mechanisms in observational data*

12 We first examine the meridional and vertical advection terms contributing to the
13 multidecadal subsurface temperature variation. Fig. 7 shows the regression of various zonal
14 mean terms onto the multidecadal AMO index in the SODA data (Note that the Ishii data do not
15 have ocean currents and cannot be used for the ocean heat budget). The similar results can be
16 obtained by computing the zonal advection terms at each grid point and then performing the
17 zonal mean and regression onto the AMO index. It is clearly seen that the TNA subsurface
18 cooling anomalies can be broadly explained by the total meridional advection (Fig. 7a), while the
19 total vertical advection plays a much smaller role except north of 14°N (Fig. 7e). The advection
20 by the ocean currents is further decomposed into two components: Anomalous (denoted by
21 prime) and mean (denoted by overbar) currents. It is shown that the total meridional advection

1 mainly arises from the advection by the anomalous meridional current ($-V'\partial\bar{T}/\partial y$, Fig. 7b),
2 whereas the advection by the mean meridional current is secondary ($-\bar{V}\partial T'/\partial y$, Fig. 7c).
3 Compared to these two terms, the nonlinear term is small ($-V'\partial T'/\partial y$, Fig. 7d). A remarkable
4 feature is that the subsurface cooling between 8°N - 20°N in Fig. 1b corresponds to the
5 contribution due to the advection term by the anomalous current in Fig. 7b ($-V'\partial\bar{T}/\partial y < 0$ in
6 the TNA subsurface ocean). Because the mean meridional temperature gradient is positive at
7 the TNA subsurface ocean ($\partial\bar{T}/\partial y > 0$, Fig. 6a), an anomalous northward current must occur in
8 the subsurface ocean, i.e., V' must be positive. Since the zonally averaged field is considered
9 here, it is expected that the anomalous northward current is associated with the flow variations of
10 the AMOC and/or the Atlantic subtropical cell (STC). We will come back this issue later.

11 Similar to the total meridional advection, the total vertical advection primarily depends on
12 the advection by the anomalous vertical velocity (Fig. 7e vs Fig. 7f), while the advection by the
13 mean vertical velocity plays a much smaller role (Fig. 7e vs Fig. 7g). The nonlinear term can
14 be ignored (Fig. 7h). The advection by the anomalous vertical velocity ($-W'\partial\bar{T}/\partial z$) tends to
15 cool temperature in the upper 400 m north of 14°N and to warm temperature south of 14°N .
16 Because $\partial\bar{T}/\partial z$ is always positive, this implies that there is an anomalous downwelling
17 (upwelling) south (north) of 14°N , consistent with the wind distribution (and its corresponded
18 Ekman transport and vertical motion) associated with the AMO (Fig. 8a). The effect of the
19 advection by the mean vertical velocity tends to be opposite to that by the anomalous vertical
20 velocity (Fig. 7g vs Fig. 7f).

1 The contributions of both $-\bar{W} \partial T' / \partial z$ and $-\bar{V} \partial T' / \partial y$ to the TNA subsurface
2 temperature cooling are small. These suggest that the anomalous temperature gradients induced
3 by the local process or remote forcing such as the thermocline adjustment (Zhang 2007) cannot
4 produce the subsurface temperature cooling on multidecadal timescales. The result does not
5 support the hypothesis by Zhang (2007) who suggested that the ocean thermocline adjustment
6 associated with the AMOC is important for the multidecadal subsurface cooling in the TNA. In
7 summary, the TNA subsurface cooling associated with the warm phase of the AMO is largely
8 attributed to the advection by the anomalous northward current. North of 14°N , the advection
9 by an anomalous upwelling also contributes to the TNA subsurface cooling.

10 Next, we examine the TNA surface warming associated with the warm phase of the AMO.
11 The total meridional advection shows a surface cooling in the TNA region (Fig. 7a). The
12 surface cooling is contributed by both the advectons of the anomalous and mean meridional
13 currents ($-V' \partial \bar{T} / \partial y$ and $-\bar{V} \partial T' / \partial y$, Figs. 7b, c). Given the surface mean states (Figs. 5, 6),
14 this indicates that there exists an anomalous surface southward current and positive SST
15 meridional gradient anomaly. The anomalous surface southward current is largely due to the
16 anomalous westerly wind-induced Ekman drift (Fig. 8a). It is also seen that there is an obvious
17 boundary to separate the surface and subsurface cold meridional advection in Fig. 7b. This
18 boundary approximately collocates with the ocean mixed layer, and has a negligible meridional
19 advection because of the nearly zero anomalous meridional current (the transition from the
20 subsurface northward to surface southward flows) and temperature gradient.

1 The total vertical advection can explain the surface warming south of 14°N (Fig. 7e) as a
2 result of an anomalous downwelling induced by the weakened trade winds. However, it tends
3 to cool the surface temperature north of 14°N due to the anomalous upwelling (Fig. 7e, f).
4 Therefore, both the meridional and vertical advection terms cannot explain the surface warming
5 in the TNA north of 14°N associated with the warm phase of the AMO. In fact, the surface
6 warming in the TNA north of 14°N is primarily due to the surface net heat flux (Fig. 8a). The
7 westerly wind anomalies associated with the warm phase of the AMO reduce the loss of
8 turbulent heat flux and then warm the surface ocean.

9 10 *c. Physical mechanisms in CMIP5 simulations*

11 As shown earlier, 12 of 18 CMIP5 models simulated the out-of-phase variation of the TNA
12 surface and subsurface ocean temperatures reasonably well. Fig. 9 shows the 12 model
13 ensemble mean of advection term regressions onto the model AMO index. Overall, the result is
14 broadly similar to that in the SODA data. In particular, the advection by anomalous meridional
15 current is a major contribution to the TNA subsurface ocean cooling (Fig. 9b). In comparison
16 with the SODA data, the advection by the mean meridional current is well organized, with the
17 TNA subsurface ocean warming and cooling south and north of 13°N, respectively (Fig. 9c).
18 The TNA subsurface cooling north of 13°N is an obvious feature in spite of a weak magnitude.
19 This indicates that the advection of the anomalous meridional temperature gradient by the mean
20 meridional current can partly contribute to the subsurface cooling in the TNA, although it is not a
21 dominant factor.

1 Like the result in the SODA data, the anomalous downwelling south of 14°N disfavors
2 (favors) the TNA subsurface cooling (surface warming), whereas the opposite is true north of
3 14°N . In the meantime, the advection by the mean vertical velocity tends to offset but cannot
4 overwhelm the effect of advection by the anomalous vertical velocity (Figs. 9f, g). As a result,
5 the total vertical advection (Fig. 9e) is mainly determined by the advection due to the anomalous
6 vertical velocity. We have to keep in mind that the contribution of the meridional advection to
7 the TNA multidecadal temperature variation is much larger than that of the vertical advection
8 (Fig. 9a vs Fig. 9e).

9 Similar to the SODA data, the model-simulated surface warming in the TNA associated with
10 the warm phase of the AMO is also largely due to the surface net heat flux induced by the
11 weakened trade winds (Fig. 10). Nearly all the models display a cyclonic wind stress and a
12 weakening of the trade winds in the North Atlantic, consistent with the 20CRv2 reanalysis.
13 Even in the models that do not well simulate the out-of-phase relationship between the TNA
14 surface and subsurface ocean temperatures, the net surface flux still tends to warm the TNA
15 surface ocean during the warm phase of the AMO (Figs. 10m-r). This suggests that the heat
16 flux is important for the surface ocean temperature in the TNA.

17 In summary, the heat budget analyses from both observational data and CMIP5 models show
18 that the anomalous northward current plays an important role in the subsurface ocean cooling
19 (warming) in the TNA associated with the warm (cold) phase of the AMO. Given that the
20 subsurface anomaly occurs from the mixed layer down to 800-1500 m, it is expected that the
21 anomalous northward current may relate to both the deep AMOC and shallow STC variability.

1 In the following sections, we will discuss the AMOC and STC relations to the TNA ocean
2 temperature variation associated with the AMO.

3

4 **5. Link of the AMO with the AMOC and STC**

5 *a. Relation to the AMOC*

6 Both the SODA data and most of CMIP5 models show that during the warm (cold) phase of
7 the AMO, the anomalous northward (southward) meridional current is responsible for the TNA
8 subsurface ocean cooling (warming). To examine AMOC relation to this variation, we first
9 calculate the AMOC streamfunctions. The long-term mean streamfunctions for the SODA data
10 and CMIP5 models are shown in Fig. 8b and Fig. 11, respectively. The mean AMOC
11 streamfunctions show highly varying structures. The positions of the maximum overturning are
12 typically found at 600-1500 m depth and between 20°N and 60°N. There are large differences
13 in how the models reproduce the lower overturning cell. Several models show either an absent
14 or a very weak lower overturning cell of the Antarctic Bottom Water (AABW), while other
15 models show the AABW all the way north to 60°N. Hydrographic observations show that the
16 AABW almost disappears north of 35°N (Johnson 2008). CMIP5 models show a long-term
17 mean overturning circulation range from 13 to 33 Sv. Based on hydrographic data, the
18 estimates of the AMOC strength are 14-18 Sv at 24°N (Ganachaud and Wunsch 2000; Lumpkin
19 and Speer 2003), 18.7 ± 5.6 Sv at 26.5°N (Cunningham et al. 2007), and 13-19 Sv at 48°N
20 (Ganachaud 2003). Generally speaking, CMIP5 models basically capture the feature of the
21 AMOC although the magnitude and location are a little bit different from observations.

1 The AMOC index in the TNA Ocean is defined as the maximum streamfunction in the
2 latitude band of 5°N-20°N. Similar results can be obtained if we choose a specific latitude in
3 the TNA (not shown). To reduce and/or exclude the surface wind driven overturning, we have
4 used a further criterion that the maximum should be located deeper than 300 m. The AMOC
5 indices in the TNA for the SODA data and CMIP5 models are shown in Fig. 8c and Fig. 12. To
6 emphasize the multidecadal variability, we have detrended and smoothed the indices by a 7-year
7 low-frequency filter. An initial impression is that these TNA AMOC indices vary differently.
8 However, a close examination finds that the TNA AMOC indices in the SODA data and most of
9 CMIP5 models vary with their individual AMO indices. The feature can be clearly seen from
10 the correlation plots in Fig. 8e and Fig. 13. At the zero time lag, the TNA AMOC and AMO
11 indices are positively correlated in the SODA data and the 12 CMIP5 models that are able to
12 simulate the TNA subsurface ocean cooling (Fig. 8e and Figs. 13a-l). For the 6 models that are
13 unable to simulate the subsurface ocean cooling, the correlations are negative except the nearly
14 zero correlation of IPSL-CM5A-MR (Figs. 13m-r). This implies that the TNA AMOC is
15 strengthened (weakened) during the warm (cold) phase of the AMO. It also means that there is
16 an anomalous northward (southward) current in the TNA upper ocean layer during the warm
17 (cold) phase of the AMO, which in turn induces the TNA subsurface cooling (warming). This
18 is consistent with the result of the heat budget analysis shown earlier for the SODA data and the
19 12 models showing realistic subsurface temperature anomalies.

20 Previous studies suggested that the AMOC variations have a latitudinal dependence (Mignot
21 and Frankignoul 2005; Msadek and Frankignoul 2009; Zhang 2010). These studies showed that

1 the subpolar AMOC variation leads the subtropical and tropical AMOC variations by several
2 years (about 5 years in GFDL_CM2.1 model) and the length of time lag is mainly determined by
3 the advection speed in the North Atlantic deep water formation region (Zhang 2010). Here, we
4 also analyze the high-low latitudinal dependence of the relationship between the AMOC and
5 AMO in CMIP5 simulations. In the higher latitudes, most of the models show that the AMOC
6 leads the AMO (not shown). As the latitude decreases, the leading time becomes smaller and
7 the relationship between the AMOC and AMO becomes more and more synchronized. Thus,
8 the warm (cold) phase of the AMO corresponds to a strengthened (weakened) TNA AMOC in
9 the nearly zero time lag.

10 The positive correlations between the AMO and TNA AMOC in the SODA data and CMIP5
11 models maximize in different ways. Some models show zero time lag (e.g., GFDL-ESM2G).
12 Some models show that the maximum correlation occurs when the TNA AMOC leads by several
13 years (e.g., GFDL-ESM2M), while the correlation in the SODA data maximizes when the AMO
14 leads the TNA AMOC by 5 years (Fig. 8e). This inconsistency may arise from the different
15 adjustment time of the TNA AMOC (determined by the advection speed) to northern Atlantic
16 deep convection. The other possibility may be from external factors' interference such as
17 aerosols.

18

19 *b. Relation to the STC*

20 The Atlantic subtropical cell (STC) is a shallow overturning cell connecting the subtropics
21 with the equatorial region of the Atlantic Ocean (e.g., Malanotte-Rizzoli et al. 2000; Zhang et al.

1 2003). Water mass that is subducted into the thermocline in the eastern subtropics of both
2 hemispheres is swept westward by the north and south equatorial currents, respectively. The
3 water mass eventually reaches to the equatorial undercurrent, drifts eastward and upwells in the
4 eastern equator. In conjunction with the surface northward Ekman current, it forms a shallow
5 (mainly in the upper ocean of 250 m) overturning cell, i.e., the Atlantic STC. To obtain the
6 Atlantic STC variability in the Northern Hemisphere, we choose two methods to define the STC
7 index. One is similar to the Pacific STC (McPhaden and Zhang 2002, 2004; Schott et al. 2007,
8 2008), which chooses the coast-to-coast transport across 9°N as an STC index. The other
9 definition is similar to the AMOC index, which is defined as the maximum streamfunction in the
10 latitude band of 5°N-20°N in the upper 200 m. Although there are some magnitude differences
11 in the two definitions, the phase variability is very similar. So we only show results from the
12 second definition in this paper. Similar results can be obtained by using the first definition, in
13 particular for the normalized STC index and correlations with the AMO index.

14 The Atlantic STC indices in the SODA data and CMIP5 models are displayed in Fig. 8d and
15 Fig. 14. The multidecadal STC variability is different from the TNA AMOC variability (Fig.
16 8c vs Fig. 8d and Fig. 12 vs Fig. 14). For the SODA data and 12 CMIP5 models which are able
17 to simulate the out-of-phase relationship between the TNA surface and subsurface temperatures,
18 the STC indices are negatively correlated with the TNA AMOC indices at the zero time lag,
19 whereas for the other 6 models the correlations are either positive or nearly zero (not shown).
20 Since we are interested in examining the contribution of the meridional current to the TNA
21 subsurface temperature variation associated with the AMO, we focus on the lead-lag correlations

1 between the AMO and STC indices. All the models and SODA data show a negative
2 correlation between the AMO and STC indices with a zero time lag (Figs. 8f, 15). This
3 indicates that the northern Atlantic STC is significantly weakened (strengthened) during the
4 warm (cold) phase of the AMO. The weakening (strengthening) of the STC is accompanied by
5 an anomalous northward (southward) current in the subsurface (about 100-200 m) and an
6 anomalous southward (northward) Ekman drift in the surface. The anomalous subsurface
7 northward current associated with the AMO produces the multidecadal subsurface cooling as
8 exhibited in Figs. 1b, f and Fig. 4, at least in the upper 200 m. Of course, the weakening of the
9 STC cannot induce the cooling anomaly in the ocean deep layer (because of its shallow feature)
10 which is due to the AMOC variation as discussed in last subsection.

11 The STC variation associated with the AMO can be explained by the surface wind variation,
12 particularly the trade winds and the associated subtropical wind stress curl (Fig. 8a and Fig. 10).
13 The weakening (strengthening) of the surface trade winds and a positive (negative) subtropical
14 wind stress curl anomaly correspond to a decrease (an increase) of the STC. This is because the
15 interior southward Sverdrup transport, which is a key element of the subsurface branch of the
16 STC, is primarily determined by the subtropical wind stress curl. Meanwhile, the surface
17 northward Ekman transport (the upper branch of the STC) is mainly determined by the strength
18 of the trade winds. Because all models and observational data show a weakening
19 (strengthening) of the trade winds and a positive (negative) subtropical wind stress curl during
20 the warm (cold) phase of the AMO, the Atlantic STC is all weakened (strengthened) as shown in
21 Figs. 15, 8f.

1
2
3
4
5
6
7
8
9
10
11
12
13
14
15
16
17
18
19
20
21

c. Interpreting subsurface cooling by the enhanced AMOC and weakened STC

As shown in previous sections, the warm (cold) phase of the AMO is accompanied by the subsurface ocean cooling (warming) in the TNA which is mainly attributed to the meridional advection by an anomalous northward (southward) in the subsurface ocean. Our analyses have further shown that the warm (cold) phase of the AMO is associated with a strengthening (weakening) of the TNA AMOC in the SODA data and 12 CMIP5 models, but the opposite is true for the other 6 CMIP5 models. The SODA data and these 12 models do show the TNA subsurface ocean cooling (warming) during the warm (cold) phase of the AMO, whereas these 6 models do not well simulate the subsurface cooling (warming). However, all 18 models and the SODA data show that the warm (cold) phase of the AMO corresponds to a weakening (strengthening) of the Atlantic STC. The strengthening (weakening) of the AMOC features an anomalous northward (southward) current in the TNA subsurface ocean, and so does the weakening (strengthening) of the STC. These suggest that both the variations of the AMOC and STC can contribute to the subsurface ocean cooling (warming), but the AMOC contribution seems to be more important.

We first consider the case for the SODA data and the 12 CMIP5 models that are able to simulate the out-of-phase variation between the TNA surface and subsurface ocean temperatures. If the ocean mixing in the deep water formation region increases, the associated high latitude AMOC strengthens (e.g., Stocker et al. 2007; Zhang et al. 2012b). Then, the AMOC signal propagates southward accompanied with the advection, coastal and equatorial Kelvin waves, and

1 Rossby waves (e.g., Zhang 2010). After several years later, the AMOC in the TNA reaches to
2 the maximum, induces an anomalous northward current in the upper 1500 m, and thus generates
3 a TNA subsurface ocean cooling between 8°N-20°N where the mean meridional temperature
4 gradient is positive due to the 9°N temperature dome. Meanwhile, at the surface the
5 strengthened AMOC leads to a substantial North Atlantic and TNA surface warming (the warm
6 phase of the AMO) as a result of the increased net heat flux and increased northward heat
7 transport. The TNA surface warming decreases the surface pressure, induces an anomalous
8 surface convergence, and thus generates a weakening of the trade winds and a positive wind
9 stress curl anomaly in the subtropical North Atlantic. On one hand, the weakened trade winds
10 tend to warm SST by decreasing the turbulent heat flux loss and increasing the Ekman drift
11 induced downwelling. On the other hand, the weakened trade winds and positive wind stress
12 curl anomaly reduce the shallow STC strength and the associated subsurface southward interior
13 current, generating an anomalous northward current. Thus, like the AMOC, the STC also acts
14 to cool the TNA subsurface ocean.

15 The situation is different for the 6 CMIP5 models that are not well simulate the out-of-phase
16 variation between the TNA surface and subsurface ocean temperatures. These models show
17 that the warm (cold) phase of the AMO is associated with a weakening (strengthening) of the
18 AMOC in the TNA. So the models cannot simulate the anomalous northward (southward)
19 current induced by the AMOC in the TNA subsurface ocean that is required for the subsurface
20 cooling (warming) during the warm (cold) phase of the AMO. However, these 6 models are
21 able to simulate the inverse relationship between the shallow STC and AMO because the STC is

1 mostly wind-driven (the models do simulate the feature of the weakened trade winds). This
2 means that the simulated warm (cold) phase of the AMO is associated with a weakening
3 (strengthening) of the STC. The weakening (strengthening) of the STC induces an anomalous
4 northward (southward) current which can make a contribution to the subsurface ocean cooling
5 (warming) in the TNA. However, this contribution is not large enough for the models to fully
6 simulate the out-of-phase variation between the subsurface and surface ocean temperatures in the
7 TNA.

8

9 **6. Multidecadal salinity variation in the TNA Ocean**

10 Given the feature of the TNA surface and subsurface temperature variation, a natural
11 question is: Does salinity show a similar variation in the TNA Ocean? Using the pentadal
12 salinity data of the World Ocean Database 2005 (Boyer et al. 2006), Wang et al. (2010) showed
13 that the salinity anomalies do not seem to display an out-of-phase relationship between the
14 surface and subsurface oceans in the TNA associated with the AMO (see their Fig. 10). Here
15 we also calculate the regressions of the Atlantic zonal mean ocean salinity onto the AMO index
16 for the SODA and Ishii data (Figs. 16s, t). The SODA regression is similar to the result of
17 Wang et al. (2010), which shows a uniform freshening in the TNA surface and subsurface oceans.
18 The Ishii salinity regression does not seem to show an obvious out-of-phase relation either
19 although there is a positive salinity regression near the surface north of 15°N (Fig. 16t). We
20 have to keep in mind that the salinity data may not be reliable, especially during earlier time.

21 The regressions of the Atlantic zonal mean ocean salinity onto their individual AMO indices

1 for the 18 CMIP5 models are shown in Figs. 16a-r. For most of the 12 models that are able to
2 simulate the multidecadal TNA temperature variation, they also produce the out-of-phase
3 relation in the TNA surface and subsurface ocean salinity (Figs. 16a-l). During the warm (cold)
4 phase of the AMO, these models show the negative salinity anomalies in the TNA subsurface
5 ocean and the positive salinity anomalies in the surface ocean. For the 6 models that are unable
6 to simulate the out-of-phase temperature variation, they cannot well produce the negative salinity
7 anomalies in the TNA subsurface ocean either (Figs. 16m-r).

8 We also calculate the salinity variation contribution by the ocean advection terms. The
9 salinity variation is largely determined by the meridional salinity advection. The 12 model
10 ensemble mean of the regressions of the meridional salinity advection terms onto the AMO index
11 is shown in Fig. 17. It is shown that the total meridional advection can explain the decreased
12 salinity in the TNA subsurface ocean and the increased salinity in the TNA surface ocean (Fig.
13 17a). A further decomposition shows that the salinity advection by the anomalous meridional
14 current plays a dominant role and the other terms are secondary (Figs. 17b-d). Given the
15 positive mean meridional salinity gradient ($\partial\bar{S}/\partial y > 0$), Fig. 17b indicates that the TNA
16 subsurface ocean has an anomalous northward current, whereas the surface ocean flow is
17 anomalously southward. These are consistent with the results in the last section that these 12
18 models are associated with a strengthening of the TNA AMOC and a weakening of the Atlantic
19 STC during the warm phase of the AMO, both of which result in an anomalous northward
20 current in the subsurface ocean. The surface anomalous southward flow is due to the Ekman
21 transport induced by the weakened trade winds associated with the warm phase of the AMO.

1 Thus, the model simulated AMOC and STC can also contribute to the salinity variation of the
2 TNA subsurface and surface oceans on multidecadal timescales.

3

4 **7. Discussion and conclusion**

5 The paper uses observational data and CMIP5 model simulations to show and examine the
6 variations of the Atlantic multidecadal oscillation (AMO), Atlantic meridional overturning
7 circulation (AMOC), subtropical cell (STC) and surface wind in the North Atlantic. It is shown
8 that the tropical North Atlantic (TNA) features an anticorrelated variation in the surface and
9 subsurface ocean temperatures associated with the AMO. That is, the warm (cold) phase of the
10 AMO is accompanied by a warm (cold) surface ocean and a cold (warm) subsurface ocean in the
11 TNA. Given that there is no significant rapid TNA subsurface response to changes in the
12 radiative forcing, this multidecadal TNA subsurface temperature anomaly can be taken as a
13 proxy or fingerprint for the AMOC variation (Zhang 2007). Here we show that the
14 anticorrelated surface and subsurface temperature variation in the TNA does indeed link with the
15 variations of both the AMOC and STC. We found that the TNA subsurface temperature
16 variation is largely attributed to the advection by the anomalous meridional current ($-V'\partial\bar{T}/\partial y$)
17 which is induced by the AMOC and STC variations. Because the mean meridional temperature
18 gradient in the TNA subsurface is positive ($\partial\bar{T}/\partial y > 0$) due to the temperature dome at 9°N,
19 the anomalous subsurface current induced by the AMOC and STC basically controls the
20 variation of the TNA subsurface temperature. The advections of the anomalous temperature

1 gradients by the mean currents ($-\bar{W} \partial T' / \partial z$ and $-\bar{V} \partial T' / \partial y$) are of secondary importance in
2 controlling the TNA subsurface temperature variation. This suggests that the temperature
3 gradient changes induced by the local process or remote forcing such as the thermocline
4 adjustment (Zhang 2007) cannot produce the subsurface temperature cooling associated with the
5 warm phase of the AMO.

6 The variations of the AMOC, STC, ocean temperature and surface wind with the AMO can
7 be summarized in Fig. 18. A strengthening of the AMOC is associated with the AMOC
8 anomaly signal in the high latitude that propagates southward, which is accompanied with the
9 advection, coastal and equator Kelvin waves, and Rossby waves (e.g., Zhang 2007). Several
10 years later, the strength of the TNA AMOC reaches to its maximum, which induces an
11 anomalous northward current in the upper ocean of 2000 m and thus generates a TNA subsurface
12 cooling between 8°N-20°N where the mean meridional temperature gradient is positive due to
13 the 9°N temperature dome. Meanwhile, in the surface, the strengthened AMOC leads to a
14 substantial North Atlantic and TNA surface warming (i.e., the warming during the warm phase
15 of the AMO). The TNA surface warming decreases the surface pressure, induces an anomalous
16 surface convergence and thus generates a weakening of the trade winds and a positive wind
17 stress curl anomaly over the subtropical North Atlantic. On one hand, the weakened trade
18 winds tend to warm the surface ocean by decreasing the turbulent heat flux loss and increasing
19 the Ekman drift induced downwelling. On the other hand, the weakened trade winds and
20 positive wind stress curl anomaly weaken the STC and the associated subsurface southward
21 interior current, generating an anomalous northward current and thus a subsurface cooling in the

1 TNA. The opposite is true for a weakening of the AMOC.

2 The mechanism is operated in the SODA data and 12 CMIP5 model simulations. In the
3 SODA data and 12 CMIP5 models, the warm (cold) phase of the AMO is associated with a
4 strengthening (weakening) of the TNA AMOC and a weakening (strengthening) of the STC,
5 both of which induce an anomalous northward (southward) subsurface current and thus cool
6 (warm) the TNA subsurface ocean. However, 6 CMIP5 models cannot simulate the anomalous
7 northward (southward) current induced by the AMOC in the TNA subsurface ocean during the
8 warm (cold) phase of the AMO. But these 6 models are able to produce a weakening
9 (strengthening) of the STC associated with the warm (cold) of the AMO because the STC is
10 mostly wind-driven (these models do simulate the feature of the weakened trade winds). The
11 weakening (strengthening) of the STC does induce an anomalous northward (southward) current
12 which can make a contribution to the subsurface ocean cooling (warming) in the TNA.
13 However, this contribution is not large enough for these 6 models to fully simulate the
14 out-of-phase variation between the subsurface and surface ocean temperatures in the TNA.
15 This suggests that the AMOC plays a more important role than the STC in the anticorrelated
16 variation of the TNA surface and subsurface ocean temperatures. In other words, a positive
17 correlation between the TNA AMOC and the AMO is required for models to simulate the
18 anomalous meridional current in the TNA subsurface ocean and then to change the subsurface
19 ocean temperature.

20 For most of the 12 CMIP5 models that are able to simulate the multidecadal TNA
21 temperature variation, they also produce an out-of-phase relation in the TNA surface and

1 subsurface ocean salinity. During the warm (cold) phase of the AMO, these models show the
2 negative salinity anomalies in the TNA subsurface ocean and the positive salinity anomalies in
3 the surface ocean. The mechanism is similar to that of the temperature variation. In these
4 models, the ocean salinity variations in the TNA are largely determined by the meridional
5 advection associated with the AMOC and STC variations.

6 The present paper shows that an anomalous meridional current in the TNA subsurface ocean
7 is required for simulating the subsurface ocean temperature and salinity variations associated
8 with the AMO. Both the AMOC and STC can contribute to the subsurface meridional current.
9 However, a quantitative separation of the meridional flows induced by the AMOC and STC is
10 difficult by analyzing the data and model outputs only. Numerical model experiments are
11 needed for addressing this issue. For example, two parallel model runs can be conducted. The
12 first run is a fully coupled model experiment. The second run is the same as the first one but
13 with a wind prescribing to the climatological wind in the TNA region. In this case, the STC
14 cannot be changed by the wind variation. By comparing these two model experiments, we can
15 obtain the relative contribution of the AMOC and STC to the anomalous meridional current in
16 the subsurface ocean. Assessing the quantitative effect of the AMOC and STC remains
17 challenge and is beyond the scope of this paper.

18 The variations of the ocean temperature in the TNA region are very important because they
19 directly affect hurricane activity in the North Atlantic (e.g., Shay et al. 2000). However, almost
20 all of previous studies on long-term hurricane variations use the SST variations only (e.g.,
21 Goldenberg et al. 2001; Wang et al. 2008). The present paper and others (Zhang 2007; Wang et

1 al. 2010) show that on multidecadal timescales the TNA surface and subsurface ocean
2 temperatures vary differently. In other words, the multidecadal temperature variations in the
3 TNA are different if we use different upper ocean layers (see Figs. 1 and 2). Thus, a caution
4 should be exercised for interpreting hurricane activity in terms of the multidecadal ocean
5 temperature variation in the TNA.

6

7 **Acknowledgement:** We thank three anonymous reviewers and the editor John Chiang for their
8 comments on the manuscript. This work was supported by grants from National Oceanic and
9 Atmospheric Administration (NOAA) Climate Program Office and the base funding of NOAA
10 Atlantic Oceanographic and Meteorological Laboratory (AOML). The findings and
11 conclusions in this report are those of the author(s) and do not necessarily represent the views of
12 the funding agency.

13

References

- 1
2 Booth, B. B. B., and Coauthors, 2012: Aerosols implicated as a prime driver of twentieth-century
3 North Atlantic climate variability. *Nature*, **484**, 228-232.
- 4 Boyer, T. P., and Coauthors, 2006: World Ocean Database 2005. NOAA Atlas NESDIS 60, U.S.
5 Government Printing Office, 190 pp.
- 6 Carton, J. A., and B. S. Giese, 2008: A reanalysis of ocean climate using Simple Ocean Data
7 Assimilation (SODA). *Mon. Wea.Rev.*, **136**, 2999–3017.
- 8 Compo, G. P., and Coauthors, 2011: The Twentieth Century Reanalysis Project. *Q. J. R.*
9 *Meteorol Soc.*, **137**, 1–28.
- 10 Corre, L., L. Terray, M. Balmaseda, A. Ribes, and A. Weaver, 2012: Can oceanic reanalyses be
11 used to assess recent anthropogenic changes and low-frequency internal variability of upper
12 ocean temperature? *Clim. Dyn.*, **38**, 877-896.
- 13 Cunningham, S. A., and Coauthors, 2007: Temporal variability for the Atlantic Meridional
14 Overturning Circulation at 26.5N. *Science*, **317**, 935–937, doi:10.1126/science.1141304.
- 15 Delworth, T. L., and M. E. Mann, 2000: Observed and simulated multidecadal variability in the
16 Northern hemisphere. *Climate Dynamics*, **16**, 661–676.
- 17 Enfield, D. B., A. M. Mestas-Nuñez, and P. J. Trimble, 2001: The Atlantic multidecadal
18 oscillation and its relation to rainfall and river flows in the continental U.S. *Geophys. Res.*
19 *Lett.*, **28**, 2077–2080.
- 20 Folland, C. K., D. E. Parker, and T. N. Palmer, 1986: Sahel rainfall and worldwide sea
21 temperatures, 1901–85. *Nature*, **320**, 602–607.
- 22 Folland, C. K., A. W. Colman, D. P. Rowell, and M. K. Davey, 2001: Predictability of northeast
23 Brazil rainfall and real-time forecast skill, 1987–98. *J Clim.*, **14**, 1937–1958.
- 24 Ganachaud, A. and C. Wunsch, 2000: Improved estimates of global ocean circulation, heat
25 transport and mixing from hydrographic data. *Nature*, **408**, 453–457.

- 1 Ganachaud, A., 2003: Large-scale mass transports, water mass formation, and diffusivities
2 estimated from World Ocean Circulation Experiment (WOCE) hydrographic data. *J.*
3 *Geophys. Res.*, **3213**, doi:10.1029/2002JC001565.
- 4 Goldenberg, S. B., C. W. Landsea, A. M. Mestas-Nuñez, and W. M. Gray, 2001: The recent
5 increase in Atlantic hurricane activity: Causes and implications. *Science*, **293**, 474– 479.
- 6 Gray, W. M., J. D. Sheaffer, and C. W. Landsea, 1997: Climate trends associated with
7 multidecadal variability of Atlantic hurricane activity, in *Hurricanes: Climate and*
8 *Socioeconomic Impacts*, edited by H. F. Diaz and R. S. Pulwarty. pp. 15– 53, Springer,
9 New York.
- 10 Hansen, J., and Coauthors, 2005: Earth’s energy imbalance: confirmation and implications.
11 *Science*, **308**, 1431-1435.
- 12 Ishii, M., M. Kimoto, K. Sakamoto, and S. I. Iwasaki, 2006: Steric sea level changes estimated
13 from historical ocean subsurface temperature and salinity analyses. *J. Oceanography.*, **62**
14 **(2)**, 155-170.
- 15 Johnson, G. C., 2008: Quantifying Antarctic Bottom Water and North Atlantic Deep Water
16 volumes. *J. Geophys. Res.*, **113**, C05027, doi:10.1029/2007JC004477.
- 17 Knight, J. R., and Coauthors, 2005: A signature of persistent natural thermohaline circulation
18 cycles in observed climate. *Geophys. Res. Lett.*, **32**, L20708, doi:10.1029/2005GL024233.
- 19 Lumpkin, R. and K. Speer, 2003: Large-scale vertical and horizontal circulation in the North
20 Atlantic Ocean. *J. Phys. Oceanogr.*, **33**, 1902–1920.
- 21 Malanotte-Rizzoli, P., K. Hedstrom, H. Arango, and D. B. Haidvogel, 2000: Water mass
22 pathways between the subtropical and tropical ocean in a climatological simulation of the
23 North Atlantic Ocean circulation. *Dyn. Atmos. Oceans*, **32**, 331– 371.
- 24 McCabe, G. J., M. A. Palecki, and J. L. Betancourt, 2004: Pacific and Atlantic Ocean influences
25 on multidecadal drought frequency in the United States. *Proc Natl Acad Sci.*, **101**,
26 4136-4141.
- 27 McPhaden, M. J., and D. Zhang, 2002: Slowdown of the meridional overturning circulation in

1 the upper Pacific Ocean. *Nature*, **415**, 603– 608.

2 McPhaden, M. J., and D. Zhang, 2004: Pacific Ocean circulation rebounds. *Geophys. Res. Lett.*,
3 **31**, L18301, doi:10.1029/2004GL020727.

4 Medhaug, I., and T. Furevik, 2011: North Atlantic 20th century multidecadal variability in
5 coupled climate models: sea surface temperature and ocean overturning circulation. *Ocean*
6 *Sci.*, **7**, 389-404.

7 Mignot, J., and C. Frankignoul, 2005: On the variability of the Atlantic meridional overturning
8 circulation, the NAO and the ENSO in the Bergen Climate Model. *J. Clim.*, **18**,
9 2361-2375.

10 Msadek, R., and C. Frankignoul, 2009: Atlantic multidecadal oceanic variability and its
11 influence on the atmosphere in a climate model. *Climate Dyn.*, **33**, 45-62.

12 Otterå, O. H., and Coauthors, 2003: The sensitivity of the present-day Atlantic meridional
13 overturning circulation to freshwater forcing. *Geophys. Res. Lett.*, **30**, 1898,
14 doi:10.1029/2003GL017578.

15 Rowell, D. P., C. K. Folland, K. Maskell, and M. N. Ward, 1995: Variability of summer rainfall
16 over tropical North-Africa (1906–92) observations and modelling. *Q J R Meteorol. Soc.*,
17 **121**, 669–704.

18 Rowell, D. P., 2003: The impact of Mediterranean SSTs on the Sahelian rainfall season. *J. Clim.*,
19 **16**, 849– 862.

20 Schott, F. A., and Coauthors, 2008: Pacific Subtropical Cell variability in the SODA 2.0.2/3
21 assimilation. *Geophys. Res. Lett.*, **35**, L10607, doi:10.1029/2008GL033757.

22 Schott, F. A., W. Wang, D. Stramma, 2007: Variability of Pacific subtropical cells in the 50-year
23 ECCO assimilation. *Geophys. Res. Lett.*, **34**, L05604, doi:10.1029/2006GL028478.

24 Shay, L. K., G. J. Goni, and P. G. Black, 2000: Effects of a Warm Oceanic Feature on Hurricane
25 Opal. *Mon. Wea. Rev.*, **128**, 1366–1383

26 Smith, T. M., R. W. Reynolds, 2004: Improved extended reconstruction of SST (1854–1997). *J*
27 *Clim.*, **17**, 2466–2477.

- 1 Stocker, T. F., A. Timmermann, M. Renold, and O. Timm, 2007: Effects of salt compensation on
2 the climate model response in simulations of large changes of the Atlantic meridional
3 overturning circulation. *J. Climate*, **20**, 5912–5928.
- 4 Sutton, R. T., and D. L. R. Hodson, 2005: Atlantic Ocean forcing of North American and
5 European summer climate. *Science*, **309**, 115–118.
- 6 Taylor, K. E., R. J. Stouffer, and G. A. Meehl, 2012: An overview of CMIP5 and the experiment
7 design. *Bull. Amer. Meteor. Soc.*, **93**, 485–498.
- 8 Terray, L., 2012: Evidence for multiple drivers of North Atlantic multidecadal climate variability.
9 *Geophys. Res. Lett.*, **39**, L19712, doi:10.1029/2012GL053046.
- 10 Ting, M., Y. Kushnir, R. Seager, and C. Li, 2009: Forced and internal twentieth-century SST
11 trends in the North Atlantic. *J. Climate*, **22**, 1469–1481.
- 12 Wang, C., S. dong, E. Munoz, 2010: Seawater density variations in the North Atlantic and the
13 Atlantic meridional overturning circulation. *Clim Dyn.*, **34**, 953-968.
- 14 Wang, C., and S.-K. Lee, 2009: Co-variability of Tropical Cyclones in the North Atlantic and the
15 Eastern North Pacific. *Geophys. Res. Lett.*, **36**, L24702, doi:10.1029/2009GL041469.
- 16 Wang, C., S. K. Lee, and D. B. Enfield, 2008: Atlantic Warm Pool acting as a link between
17 Atlantic Multidecadal Oscillation and Atlantic tropical cyclone activity. *Geochem. Geophys.*
18 *Geosyst.*, **9**, Q05V03 doi:10.1029/2007GC001809.
- 19 Wang, C., S. Dong, A. T. Evan, G.R. Foltz, and S.-K. Lee, 2012: Multidecadal covariability of
20 North Atlantic sea surface temperature, African dust, Sahel rainfall and Atlantic hurricanes.
21 *J. Climate*, **25**, 5404-5415.
- 22 Wang, C., L. Zhang, and S.-K. Lee, 2013: Response of freshwater flux and sea surface salinity to
23 variability of the Atlantic warm pool. *J. Climate*, in press.
- 24 Zhang, D., M. J. McPhaden, and W. E. Johns, 2003: Observational evidence for flow between
25 the subtropical and tropical Atlantic: The Atlantic subtropical cells. *J. Phys. Oceanogr.*, **33**,
26 1783–1797.
- 27 Zhang, L., C. Wang, and L. Wu, 2012a: Low-frequency modulation of the Atlantic warm pool by

1 the Atlantic multidecadal oscillation. *Climate Dynamics*, **39**, 1661–1671.

2 Zhang, L., L. Wu, and J. Zhang, 2012b: Simulated response to recent freshwater flux change
3 over the Gulf Stream and its extension: Coupled ocean–atmosphere adjustment and
4 Atlantic–Pacific teleconnection. *J. Climate*, **24**, 15, 3971–3988.

5 Zhang, R., 2007: Anticorrelated multidecadal variations between surface and subsurface tropical
6 North Atlantic. *Geophys. Res. Lett.*, **34**, L12713, doi:10.1029/2007GL030225.

7 Zhang, R., 2010: Latitudinal dependence of Atlantic Meridional Overturning Circulation
8 (AMOC) variations. *Geophys. Res. Lett.*, **37**, L16703, doi:10.1029/2010GL044474.

9 Zhang, R., and Coauthors, 2013: Have aerosols caused the observed Atlantic multidecadal
10 variability? *J. Atmos. Sci.*, in press.

11

12

1

2 Table 1. The 18 CMIP5 models used in this study.

Sponsor, Country	Model Name	Temporal Coverage
Beijing Climate Center, China	bcc-csm1-1	1850/01-2012/12
Canadian Center for Climate Modeling and Analysis, Canada	CanESM2	1850/01-2005/12
National Center for Atmospheric Research (NCAR), USA	CCSM4	1850/01-2005/12
Météo-France/Centre National de Recherches Météorologiques, France	CNRM-CM5	1850/01-2005/12
Commonwealth Scientific and Industrial Research Organisation (CSIRO), Australia	CSIRO-Mk3-6-0	1850/01-2005/12
Institute of Atmospheric Physics, Chinese Academy of Sciences, China	FGOALS-g2	1900/01-2005/12
U.S. Department of Commerce/National Oceanic and Atmospheric Administration (NOAA)/Geophysical Fluid Dynamics Laboratory (GFDL), USA	GFDL-ESM2G	1861/01-2005/12
	GFDL-ESM2M	1861/01-2005/12
National Aeronautics and Space Administration (NASA)/Goddard Institute for Space Studies (GISS), USA	GISS-E2-H	1850/01-2005/12
	GISS-E2-R	1850/01-2005/12
Met office Hadley Centre, UK	HadGEM2-ES	1859/12-2005/11
Institute Pierre Simon Laplace, France	IPSL-CM5A-LR	1850/01-2005/12
	IPSL-CM5A-MR	1850/01-2005/12
Center for Climate System Research (University of Tokyo), National Institute for Environmental Studies, and Frontier Research Center for Global Change (JAMSTEC), Japan	MIROC5	1850/01-2005/12
	MIROC-ESM	1850/01-2005/12
	MIROC-ESM-CHEM	1850/01-2005/12
Max Planck Institute for Meteorology, Germany	MPI-ESM-P	1850/01-2005/12
Meteorological Research Institute, Japan	MRI-CGCM3	1850/01-2005/12

3

4

Figure Captions

Figure 1. Variations of ocean temperature in the North Atlantic. Shown are the normalized (by standard deviation) AMO index from the (a) SODA and (e) Ishii data, the regression ($^{\circ}\text{C}$) of the Atlantic zonal mean temperature onto the normalized AMO index from the (b) SODA and (f) Ishii data, and regression ($^{\circ}\text{C}$ per $^{\circ}\text{C}$) of the Atlantic temperature averaged in the region of 8°N - 20°N and coast to coast at each depth onto the SST on multidecadal (period of T higher than 7 years) and interannual (period of T lower than 7 years) timescales from the (c, d) SODA data, and (g, h) Ishii data. The AMO is defined by the detrended SST anomalies averaged in the North Atlantic Ocean (0° to 60°N , coast to coast) and smoothed by a 7-year low-frequency filter.

Figure 2. Multidecadal time series of TNA (8°N to 20°N , coast to coast) ocean temperature anomalies at the sea surface and 200 m and vertically averaged temperature anomalies from 0-400 m using the (a, b, c) SODA and (d, e, f) Ishii data. All time series are normalized by their standard deviations.

Figure 3. The AMO indices in observation (ERSST) and CMIP5 models. The AMO index ($^{\circ}\text{C}$) is calculated by the detrended SST anomalies averaged in the North Atlantic Ocean (0° to 60°N , coast to coast) and smoothed by a 7-year low-frequency filter.

Figure 4. Regression of the Atlantic zonal mean temperature ($^{\circ}\text{C}$) onto the normalized AMO index from CMIP5 models.

Figure 5. Long-term mean background states in the TNA. The mean (a) surface wind (m/s) and net heat flux (positive downward, W/m^2) and (b) freshwater flux (evaporation minus precipitation, mm/day) are from the 20CRv2 data. The zonal (coast to coast) mean (c) temperature ($^{\circ}\text{C}$), (d) salinity (psu), (e) meridional velocity (10^{-2} m/s) and (f) vertical velocity

1 (10^{-6} m/s) are from the SODA data.

2

3 **Figure 6.** Long-term mean (a) meridional temperature gradient (10^{-6} °C/m), (b) meridional
4 salinity gradient (10^{-6} psu/m), (c) vertical temperature gradient (10^{-2} °C/m), and (d) vertical
5 salinity gradient (10^{-2} psu/m) from the SODA data.

6

7 **Figure 7.** Regression of advection terms (10^{-8} °C/s) onto the normalized AMO index from the
8 SODA data. Show are the (a) total meridional temperature advection, (b) advection by the
9 anomalous meridional current, (c) advection by the mean meridional current, and (d) nonlinear
10 term. (e-h) are the same as (a-d) but for the vertical temperature advection. The gray line in
11 (b) denotes the mean mixed layer depth, defined by the depth where the difference with the
12 potential density at the first layer equals to 0.125 kg m^{-3} .

13

14 **Figure 8.** (a) Regression of surface net heat flux (shading, positively downward, W/m^2), wind
15 stress (vector, N/m^2) and wind stress curl (contour, contour interval is $1.0 \times 10^{-9} \text{ N/m}^3$, positive
16 and negative values are denoted by the green and gray lines, respectively) onto the normalized
17 AMO index, (b) long-term mean AMOC streamfunction (S_v), (c) the TNA AMOC index, (d) the
18 STC index, lead-lag correlations of the AMO with (e) the TNA AMOC index and (f) the STC
19 index. In (e) and (f), the unit in x-axis is year, and positive (negative) year indicates the
20 AMOC/STC leads (lags) the AMO. The horizontal dash lines represent the 90% confidence
21 level. The AMO and streamfunction are from the SODA data, and the heat flux and wind are
22 from 20CRv2 reanalysis. The TNA AMOC index is defined as the maximum streamfunction
23 below 300 m between 5°N to 20°N , and the STC index is defined as the maximum
24 streamfunction in the upper 250 m between 5°N to 20°N .

25

26 **Figure 9.** Regression of advection terms (10^{-8} °C/s) onto the normalized AMO index. The
27 regression is the ensemble mean of 12 CMIP5 models that simulate the TNA surface and

1 subsurface temperature variation reasonably well. Show are the (a) total meridional
2 temperature advection, (b) advection by the anomalous meridional current, (c) advection by the
3 mean meridional current, and (d) nonlinear term. (e-h) are the same as (a-d) but for the vertical
4 temperature advection.

5
6 **Figure 10.** Regression of surface net heat flux (shading, positively downward, W/m^2), wind
7 stress (vector, N/m^2) and wind stress curl (contour, contour interval is $1.0 \times 10^{-9} \text{ N/m}^3$, positive
8 and negative values are denoted by the green and gray lines, respectively) onto the corresponding
9 normalized AMO index in CMIP5 models.

10

11 **Figure 11.** Long-term mean AMOC streamfunction (S_v) from CMIP5 models.

12

13 **Figure 12.** The TNA AMOC index defined as the maximum streamfunction below 300 m from
14 5°N to 20°N from CMIP5 models. All time series are normalized by their standard deviation.

15

16 **Figure 13.** Lead-lag correlations between the AMO and TNA AMOC index from CMIP5
17 models. The unit in x-axis is year. Positive (negative) year in x-axis means the AMOC leads
18 (lags) the AMO. The horizontal dash line indicates the 90% confidence level.

19

20 **Figure 14.** The Atlantic STC index defined as the maximum streamfunction in the upper 250
21 m between 5°N to 20°N from CMIP5 models. All time series are normalized by their standard
22 deviation.

23

24 **Figure 15.** Lead-lag correlations between the AMO and STC index from CMIP5 models.
25 The unit in x-axis is year. Positive (negative) year in x-axis means the STC leads (lags) the
26 AMO. The horizontal dash line indicates the 90% confidence level.

27

1 **Figure 16.** Regression of the Atlantic zonal mean salinity (psu) onto the normalized AMO
2 index from (a-r) CMIP5 models, (s) SODA data and (t) Ishii data.

3

4 **Figure 17.** Regression of salinity advection terms (10^{-8} psu/s) onto the normalized AMO index.
5 The regression is the ensemble mean of 12 CMIP5 models that simulate the TNA surface and
6 subsurface temperature variation reasonably well. Show are the (a) total meridional salinity
7 advection, (b) advection by the anomalous meridional current, (c) advection by the mean
8 meridional current, and (d) nonlinear term.

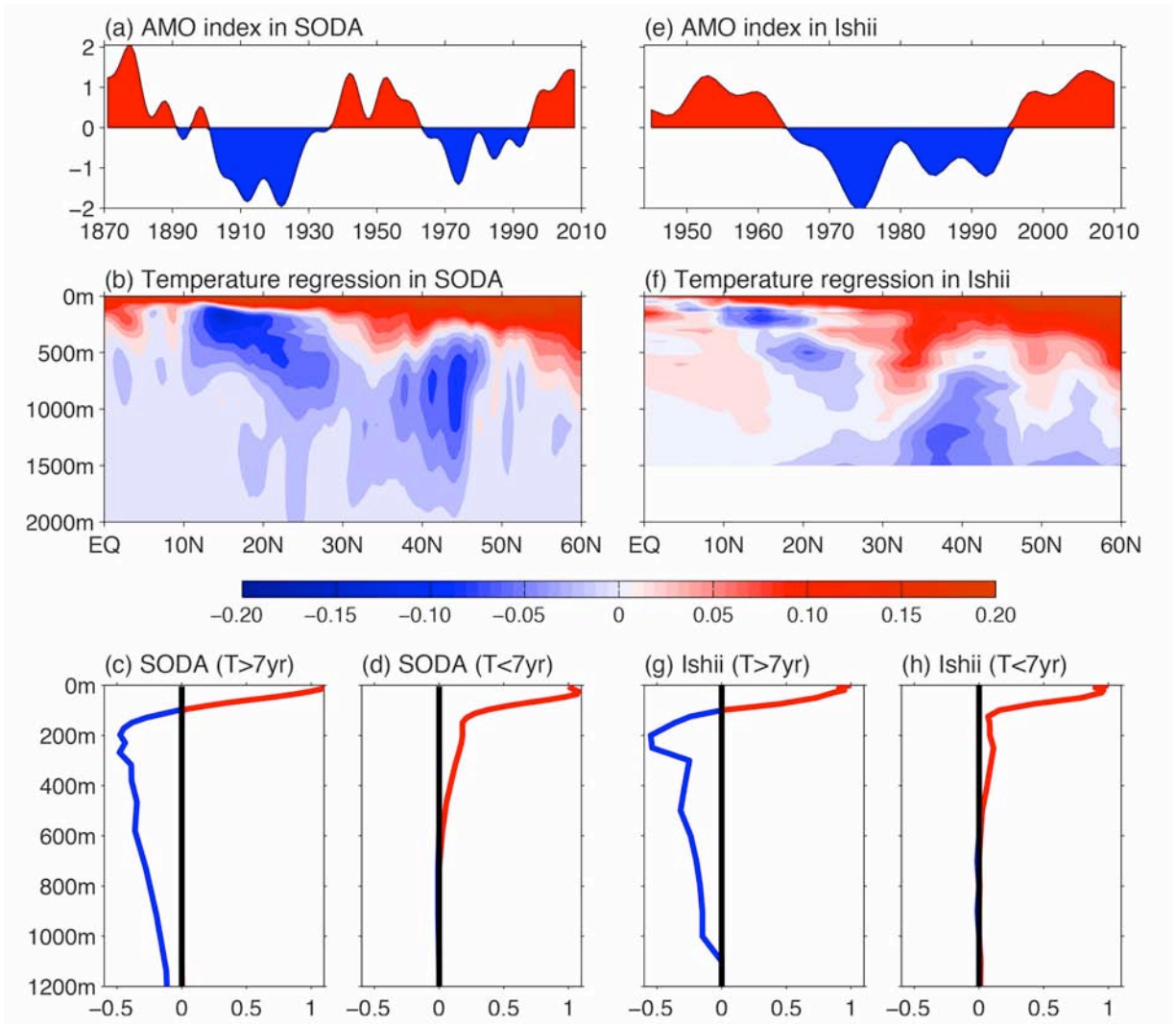
9

10 **Figure 18.** Schematic diagram showing the variations of the AMOC, STC, ocean temperature
11 and surface wind with the AMO on multidecadal timescales.

12

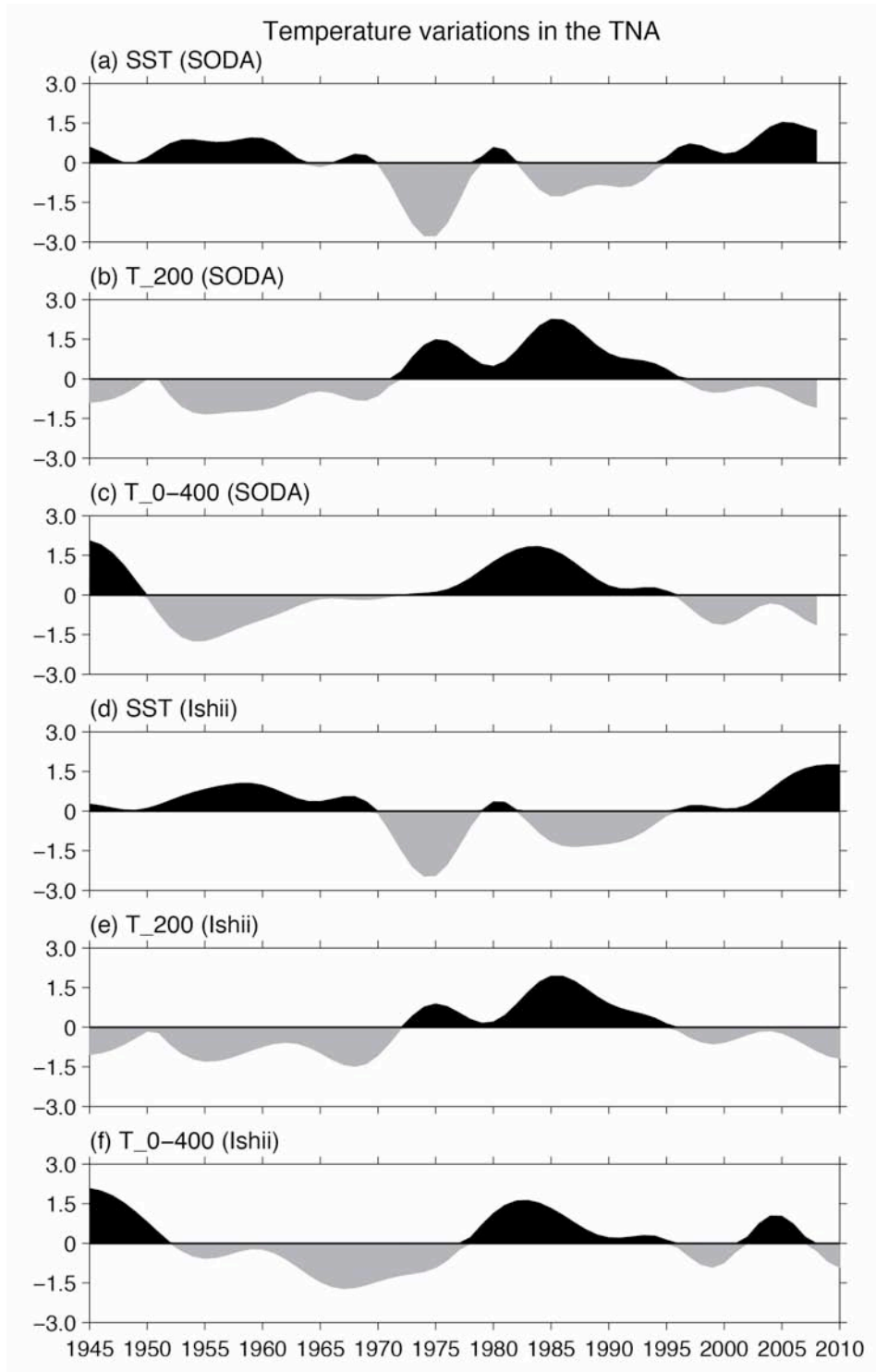
13

1
2
3



4
5
6
7
8
9
10
11
12
13

Figure 1. Variations of ocean temperature in the North Atlantic. Shown are the normalized (by standard deviation) AMO index from the (a) SODA and (e) Ishii data, the regression ($^{\circ}\text{C}$) of the Atlantic zonal mean temperature onto the normalized AMO index from the (b) SODA and (f) Ishii data, and regression ($^{\circ}\text{C per }^{\circ}\text{C}$) of the Atlantic temperature averaged in the region of 8°N - 20°N and coast to coast at each depth onto the SST on multidecadal (period of T higher than 7 years) and interannual (period of T lower than 7 years) timescales from the (c, d) SODA data, and (g, h) Ishii data. The AMO is defined by the detrended SST anomalies averaged in the North Atlantic Ocean (0° to 60°N , coast to coast) and smoothed by a 7-year low-frequency filter.



1
2
3
4
5
6

Figure 2. Multidecadal time series of TNA (8°N to 20°N, coast to coast) ocean temperature anomalies at the sea surface and 200 m and vertically averaged temperature anomalies from 0-400 m using the (a, b, c) SODA and (d, e, f) Ishii data. All time series are normalized by their standard deviations.

1
2
3

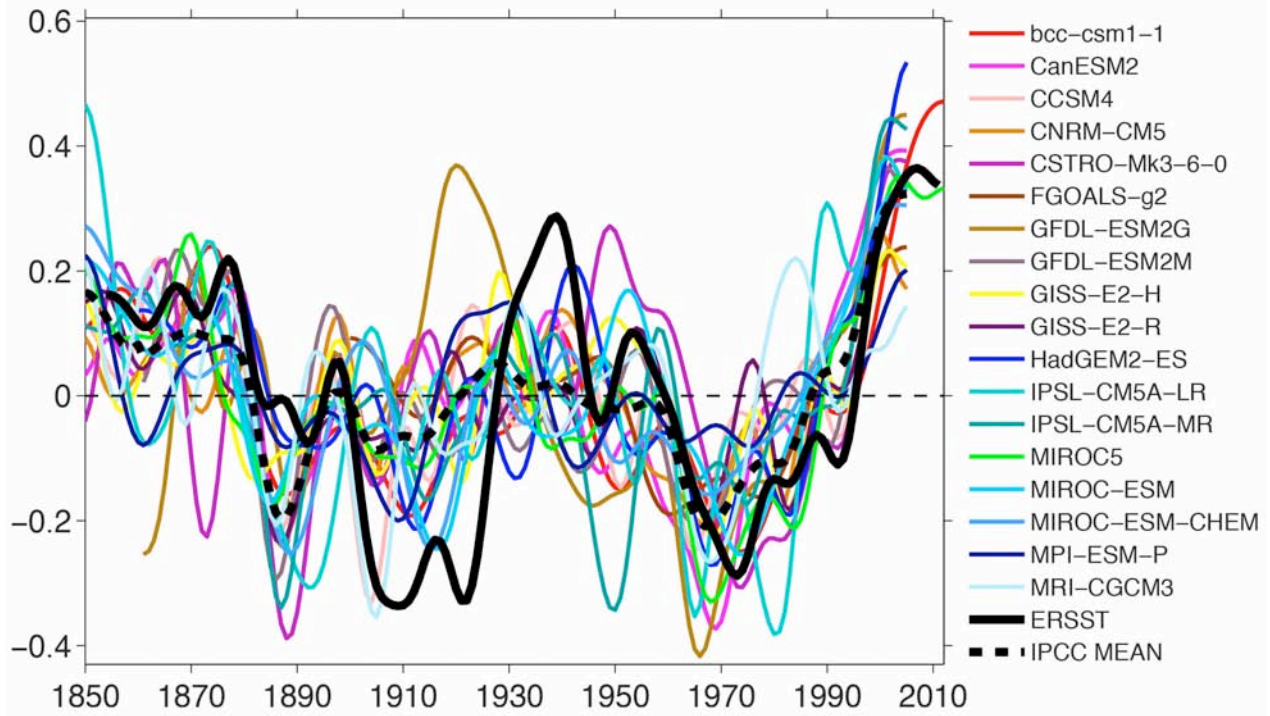
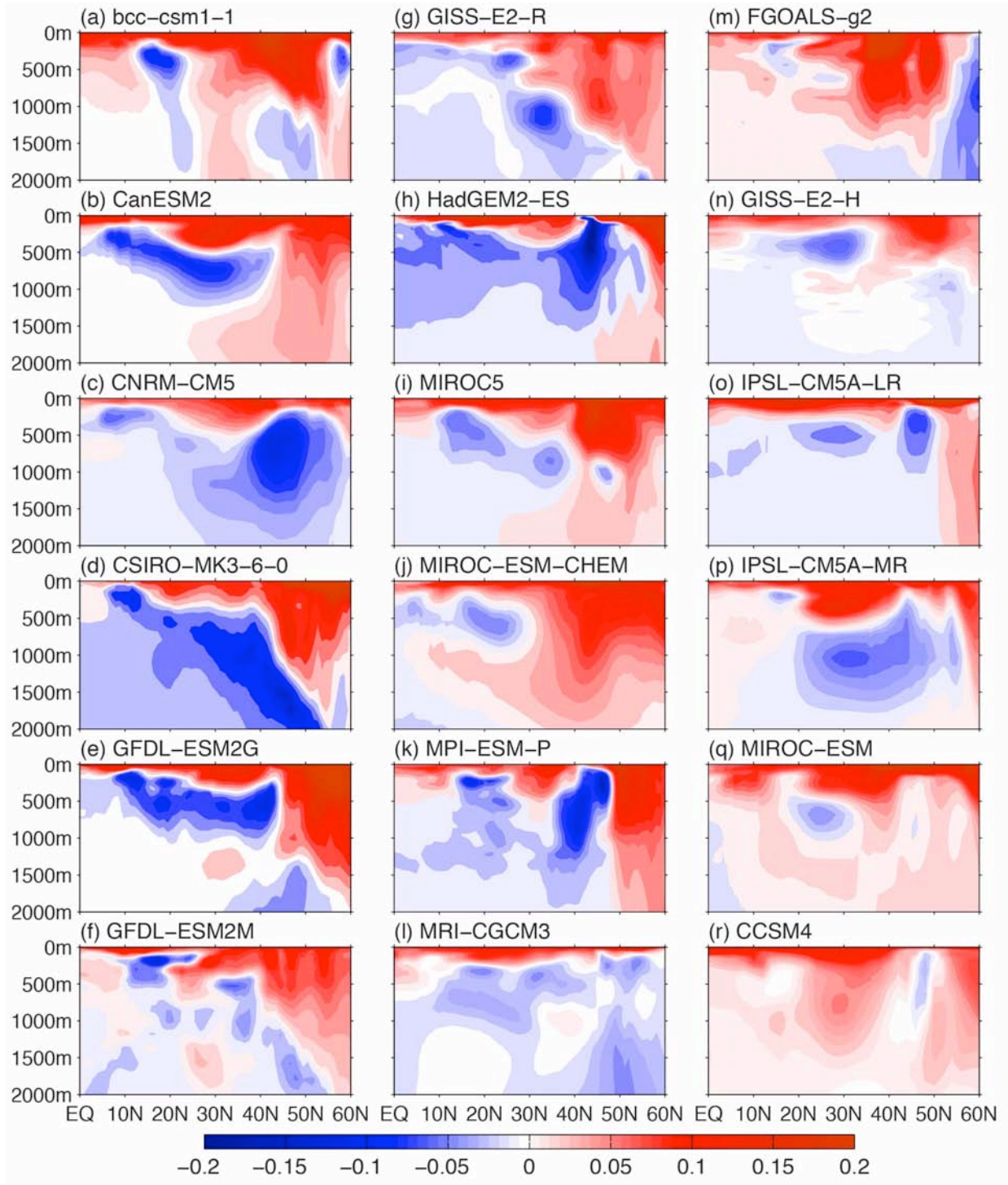


Figure 3. The AMO indices in observation (ERSST) and CMIP5 models. The AMO index ($^{\circ}\text{C}$) is calculated by the detrended SST anomalies averaged in the North Atlantic Ocean (0° to 60°N , coast to coast) and smoothed by a 7-year low-frequency filter.

1



2

3

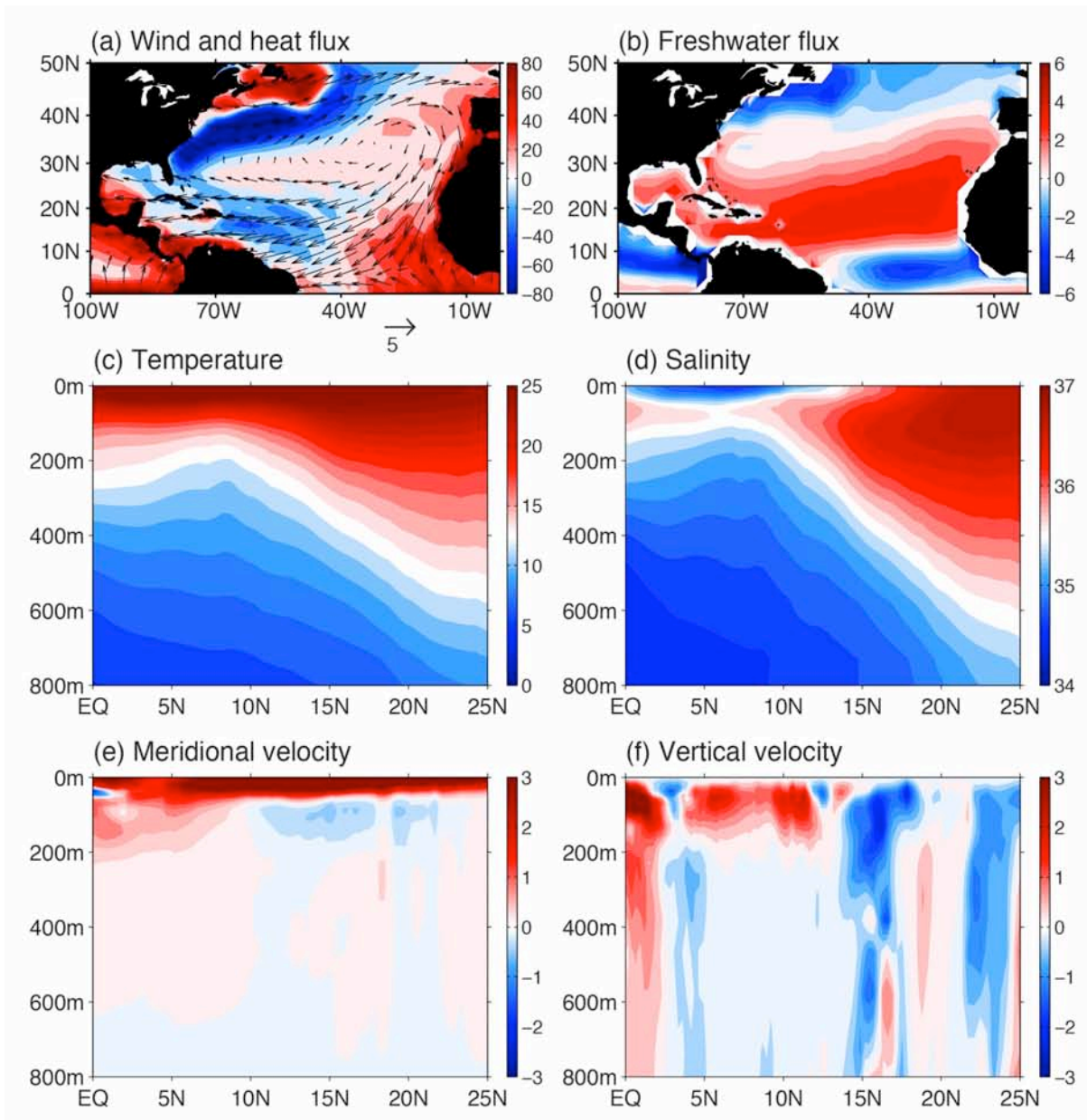
4

5

6

Figure 4. Regression of the Atlantic zonal mean temperature (°C) onto the normalized AMO index from CMIP5 models.

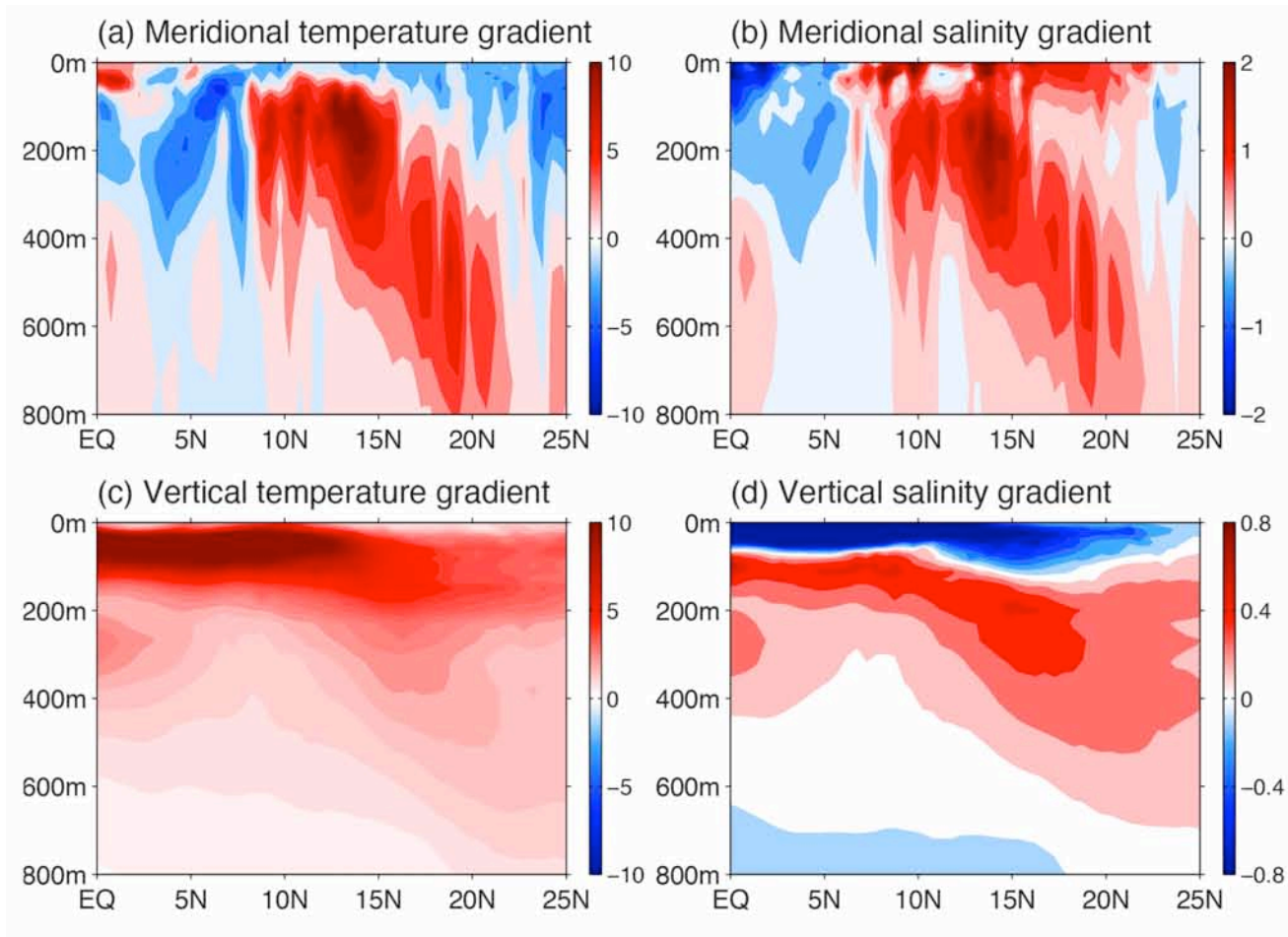
1



2
3
4
5
6
7
8

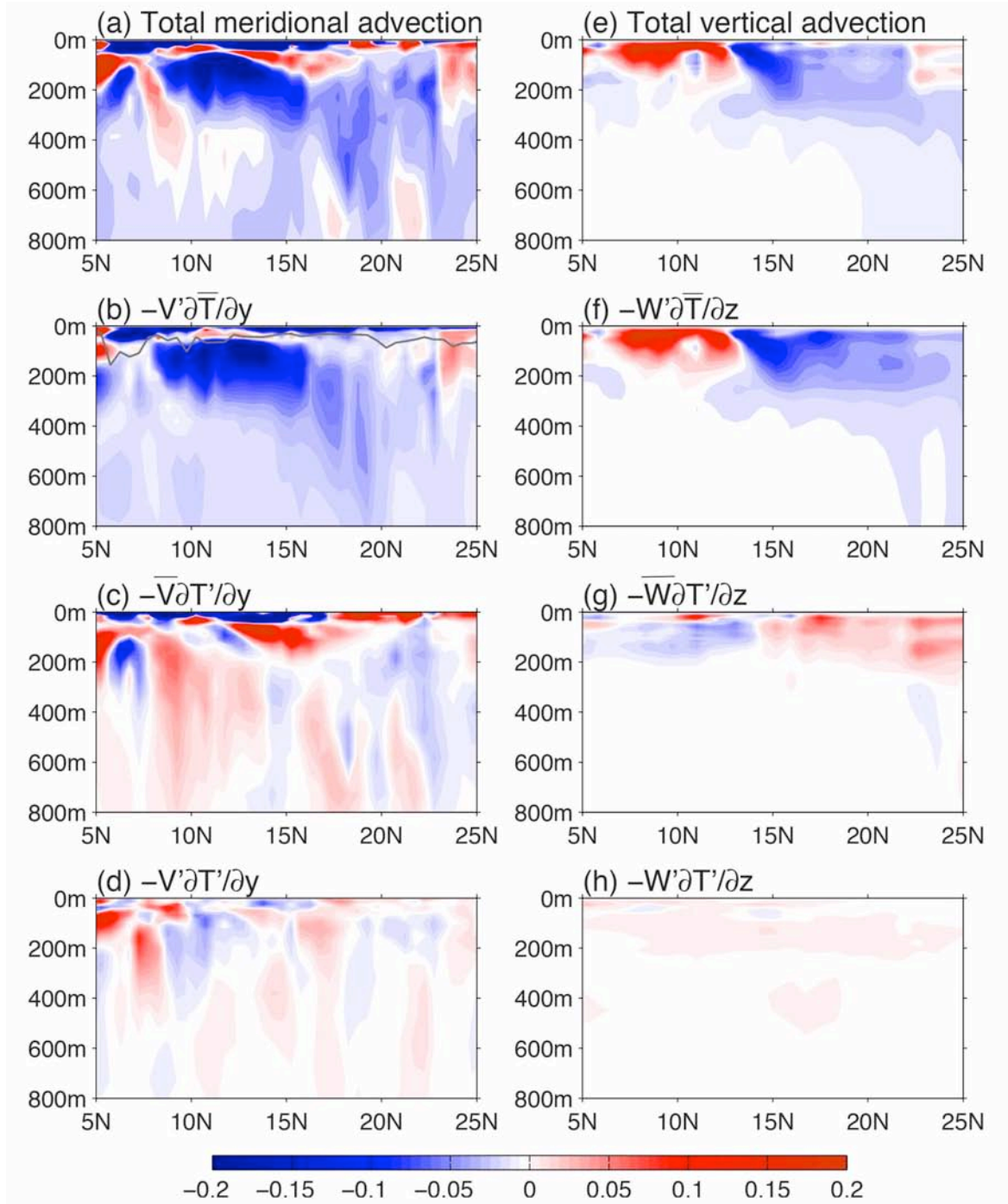
Figure 5. Long-term mean background states in the TNA. The mean (a) surface wind (m/s) and net heat flux (positive downward, W/m^2) and (b) freshwater flux (evaporation minus precipitation, mm/day) are from the 20CRv2 data. The zonal (coast to coast) mean (c) temperature ($^{\circ}\text{C}$), (d) salinity (psu), (e) meridional velocity (10^{-2} m/s) and (f) vertical velocity (10^{-6} m/s) are from the SODA data.

1
2
3
4



5
6
7
8
9
10

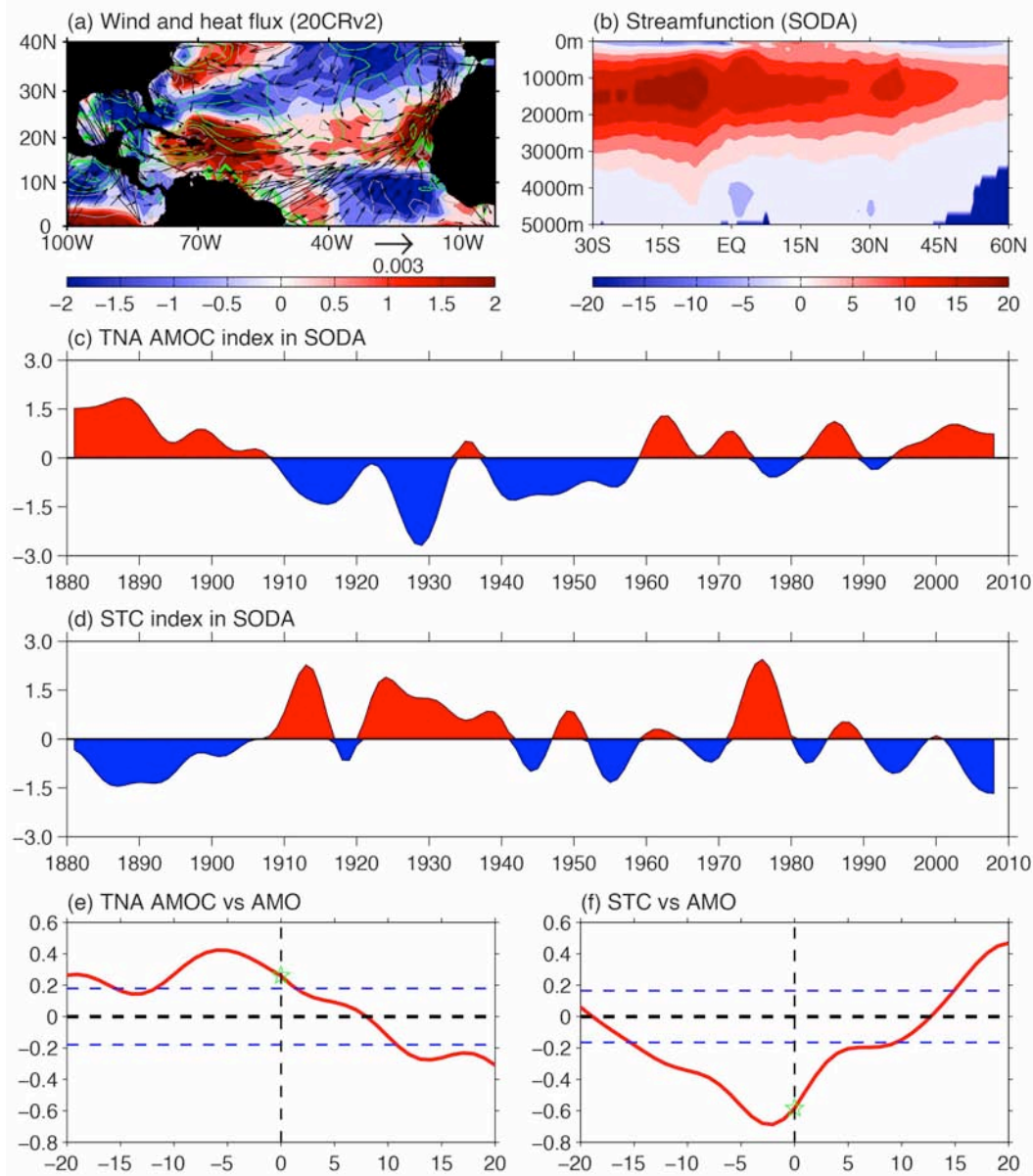
Figure 6. Long-term mean (a) meridional temperature gradient ($10^{-6} \text{ } ^\circ\text{C/m}$), (b) meridional salinity gradient (10^{-6} psu/m), (c) vertical temperature gradient ($10^{-2} \text{ } ^\circ\text{C/m}$), and (d) vertical salinity gradient (10^{-2} psu/m) from the SODA data.



1
2
3
4
5
6
7
8
9

Figure 7. Regression of advection terms ($10^{-8} \text{ }^\circ\text{C/s}$) onto the normalized AMO index from the SODA data. Show are the (a) total meridional temperature advection, (b) advection by the anomalous meridional current, (c) advection by the mean meridional current, and (d) nonlinear term. (e-h) are the same as (a-d) but for the vertical temperature advection. The gray line in (b) denotes the mean mixed layer depth, defined by the depth where the difference with the potential density at the first layer equals to 0.125 kg m^{-3} .

1

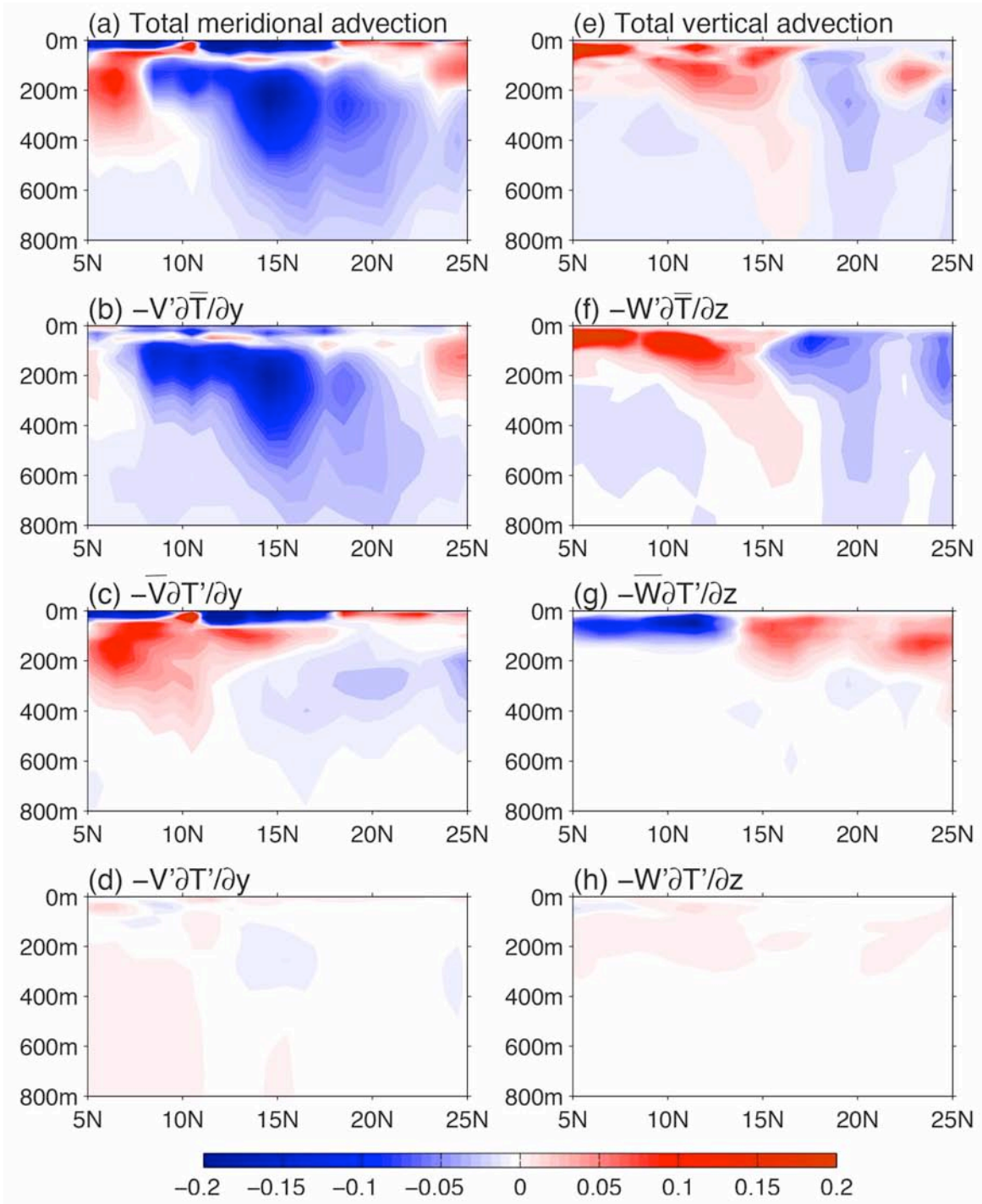


2

3

4 **Figure 8.** (a) Regression of surface net heat flux (shading, positively downward, W/m^2), wind stress (vector, N/m^2)
 5 and wind stress curl (contour, contour interval is $1.0 \times 10^{-9} N/m^3$, positive and negative values are denoted by the
 6 green and gray lines, respectively) onto the normalized AMO index, (b) long-term mean AMOC streamfunction (Sv),
 7 (c) the TNA AMOC index, (d) the STC index, lead-lag correlations of the AMO with (e) the TNA AMOC index and
 8 (f) the STC index. In (e) and (f), the unit in x-axis is year, and positive (negative) year indicates the AMOC/STC
 9 leads (lags) the AMO. The horizontal dash lines represent the 90% confidence level. The AMO and
 10 streamfunction are from the SODA data, and the heat flux and wind are from 20CRv2 reanalysis. The TNA
 11 AMOC index is defined as the maximum streamfunction below 300 m between $5^\circ N$ to $20^\circ N$, and the STC index is
 12 defined as the maximum streamfunction in the upper 250 m between $5^\circ N$ to $20^\circ N$.

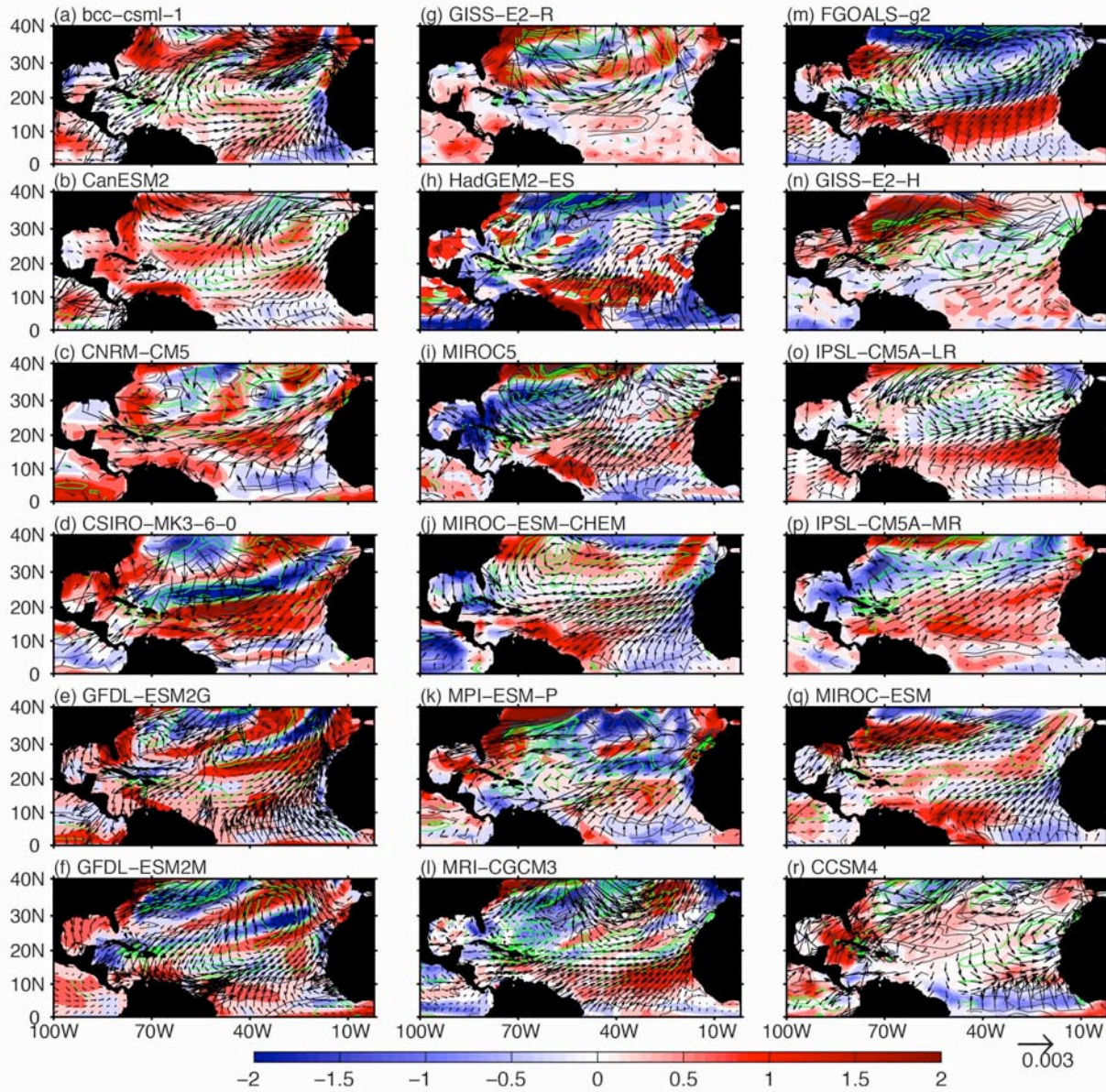
13



1
2
3
4
5
6
7
8

Figure 9. Regression of advection terms ($10^{-8} \text{ }^\circ\text{C/s}$) onto the normalized AMO index. The regression is the ensemble mean of 12 CMIP5 models that simulate the TNA surface and subsurface temperature variation reasonably well. Show are the (a) total meridional temperature advection, (b) advection by the anomalous meridional current, (c) advection by the mean meridional current, and (d) nonlinear term. (e-h) are the same as (a-d) but for the vertical temperature advection.

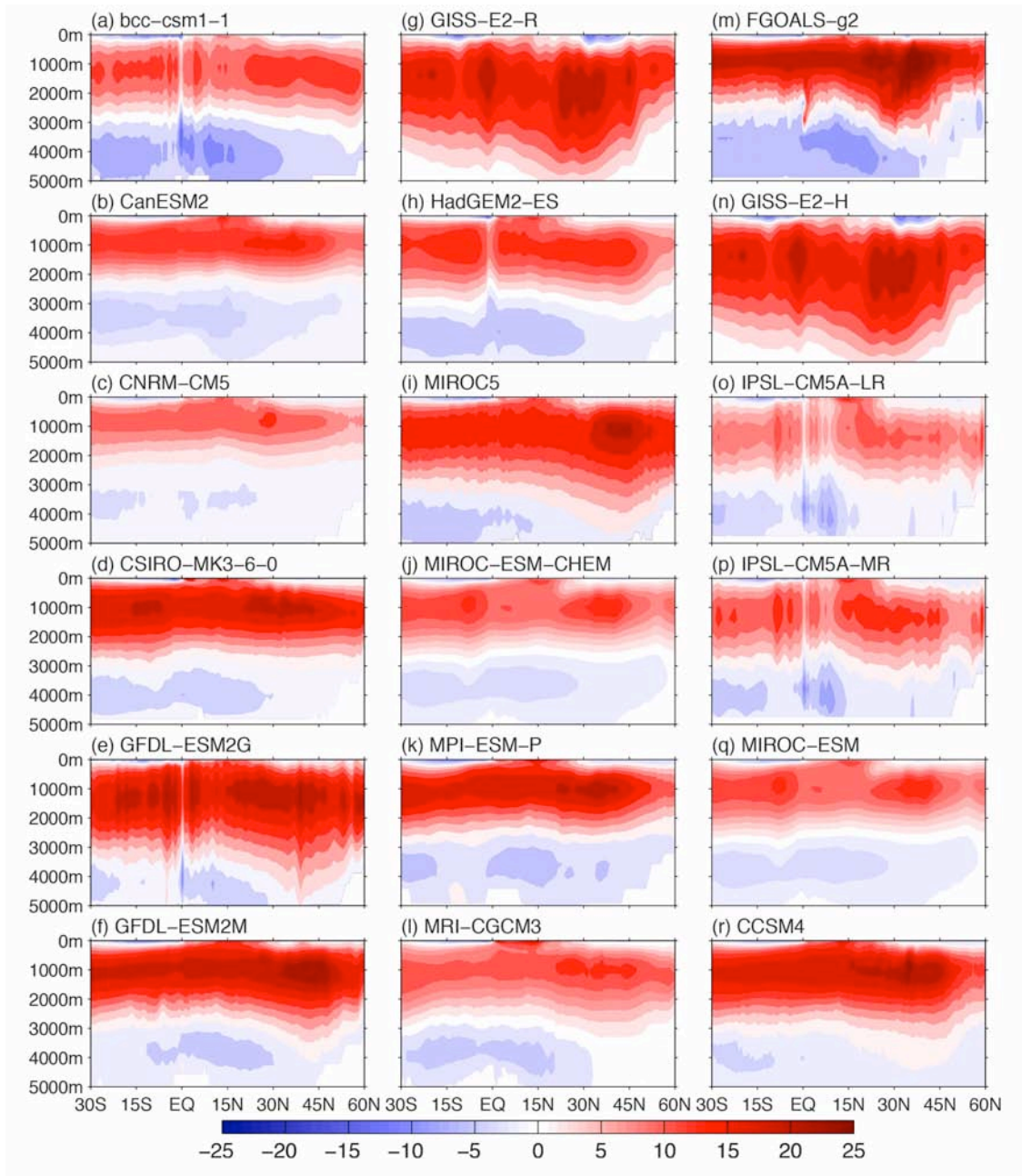
1
2



3
4
5
6
7
8

Figure 10. Regression of surface net heat flux (shading, positively downward, W/m^2), wind stress (vector, N/m^2) and wind stress curl (contour, contour interval is $1.0 \times 10^{-9} \text{ N/m}^3$, positive and negative values are denoted by the green and gray lines, respectively) onto the corresponding normalized AMO index in CMIP5 models.

1



2

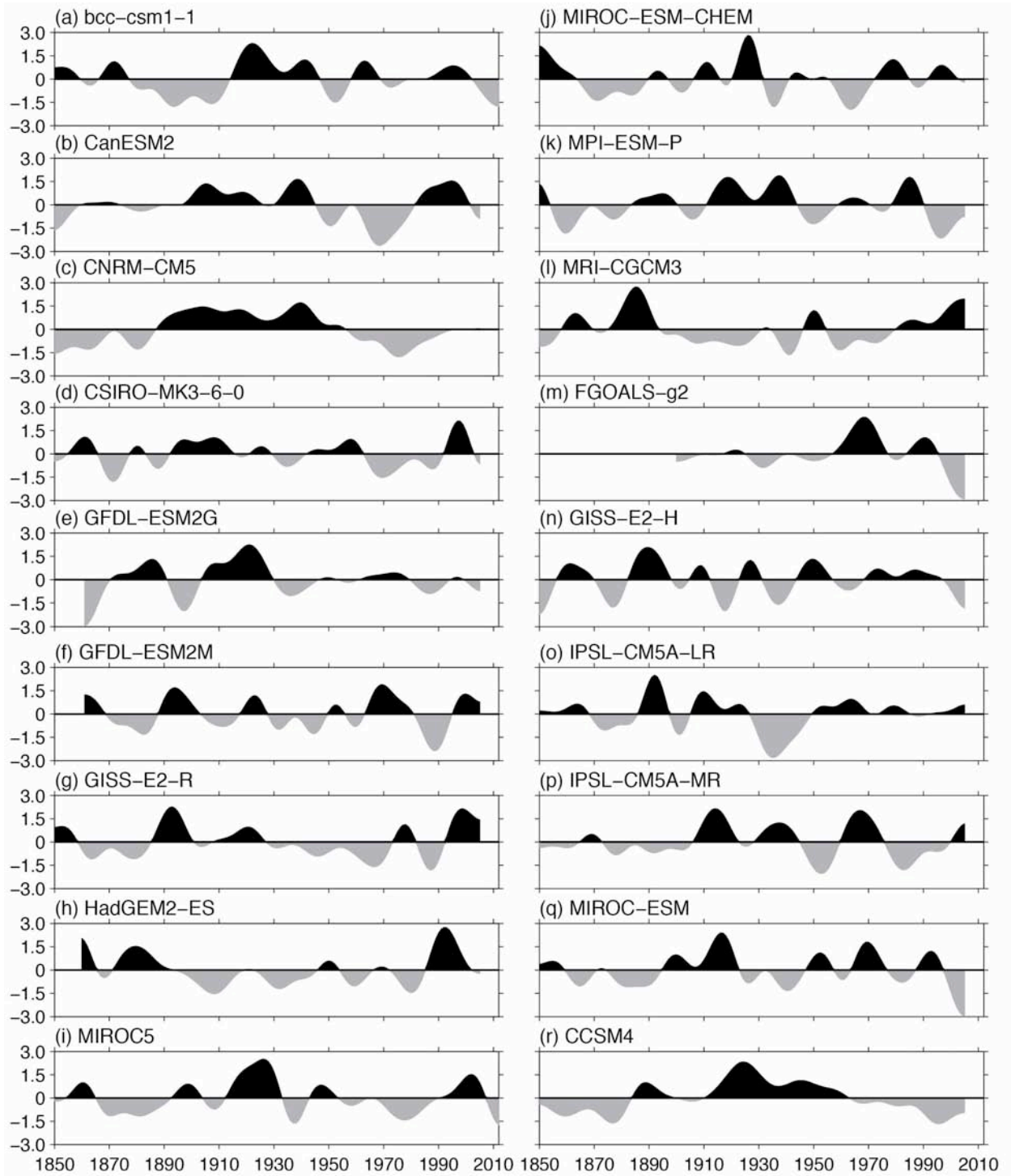
3

4

Figure 11. Long-term mean AMOC streamfunction (Sv) from CMIP5 models.

5

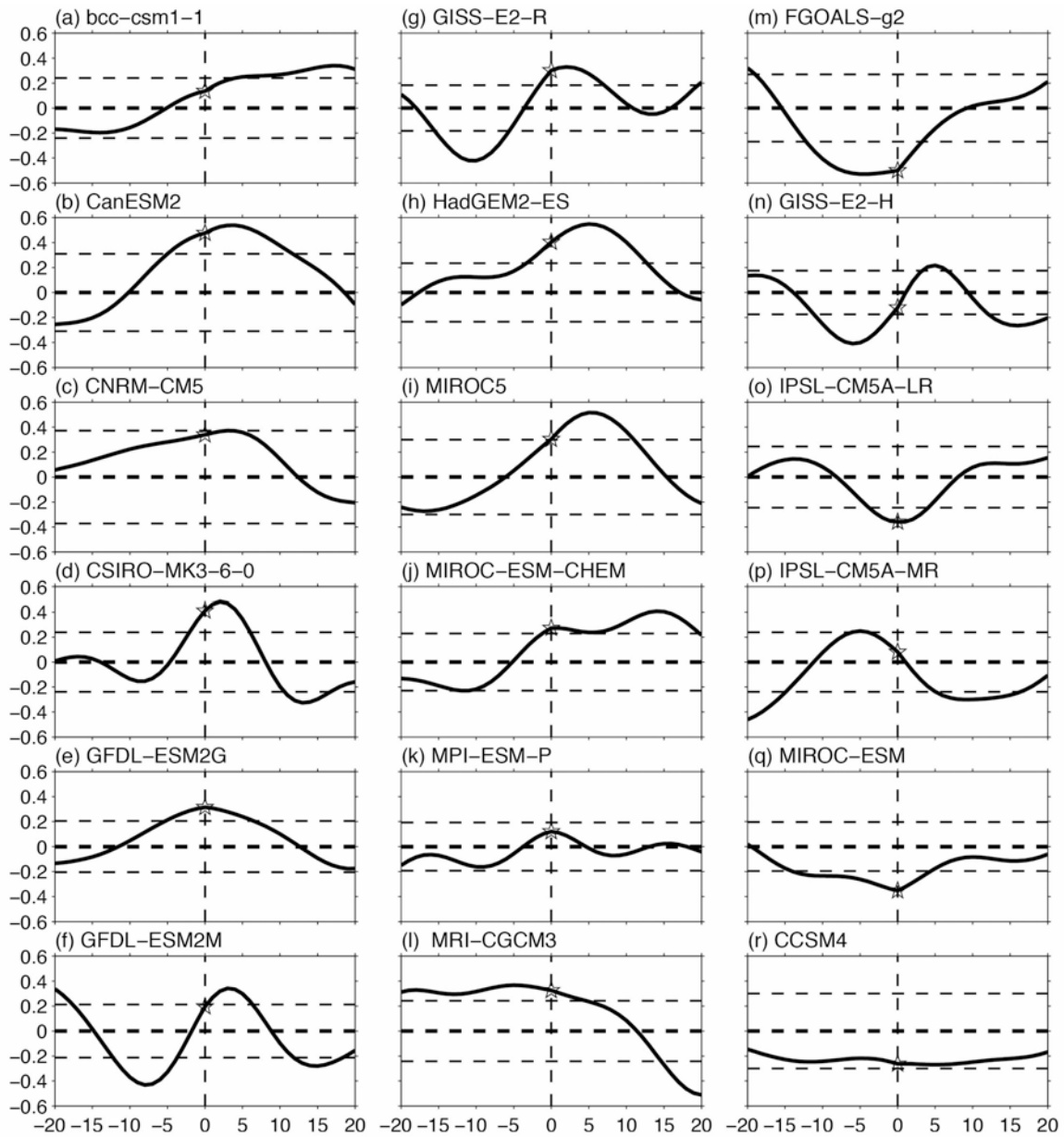
1



2
3
4
5
6

Figure 12. The TNA AMOC index defined as the maximum streamfunction below 300 m from 5°N to 20°N from CMIP5 models. All time series are normalized by their standard deviation.

1



2

3

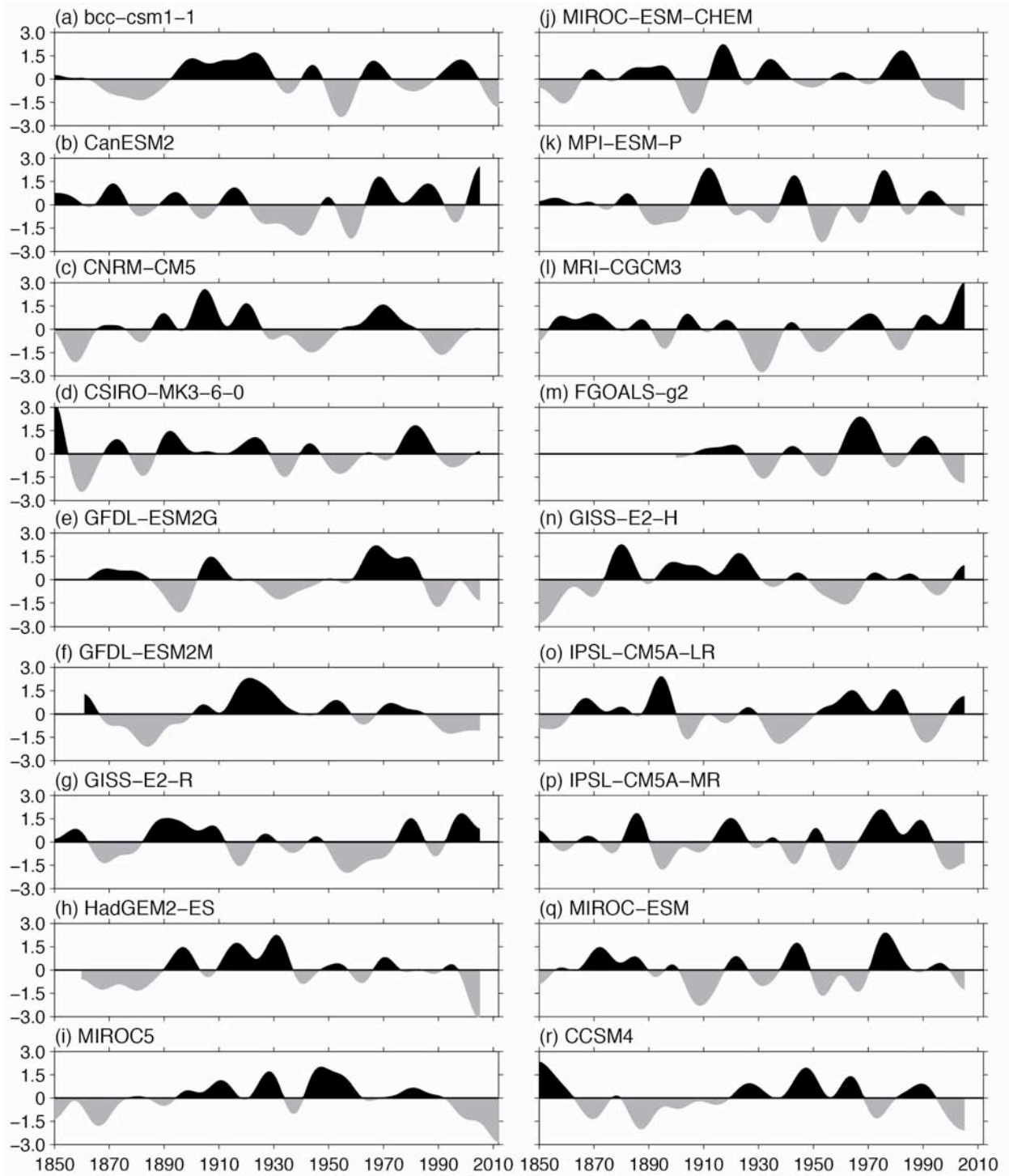
4 **Figure 13.** Lead-lag correlations between the AMO and TNA AMOC index from CMIP5 models. The unit in

5 x-axis is year. Positive (negative) year in x-axis means the AMOC leads (lags) the AMO. The horizontal dash

6 line indicates the 90% confidence level.

7

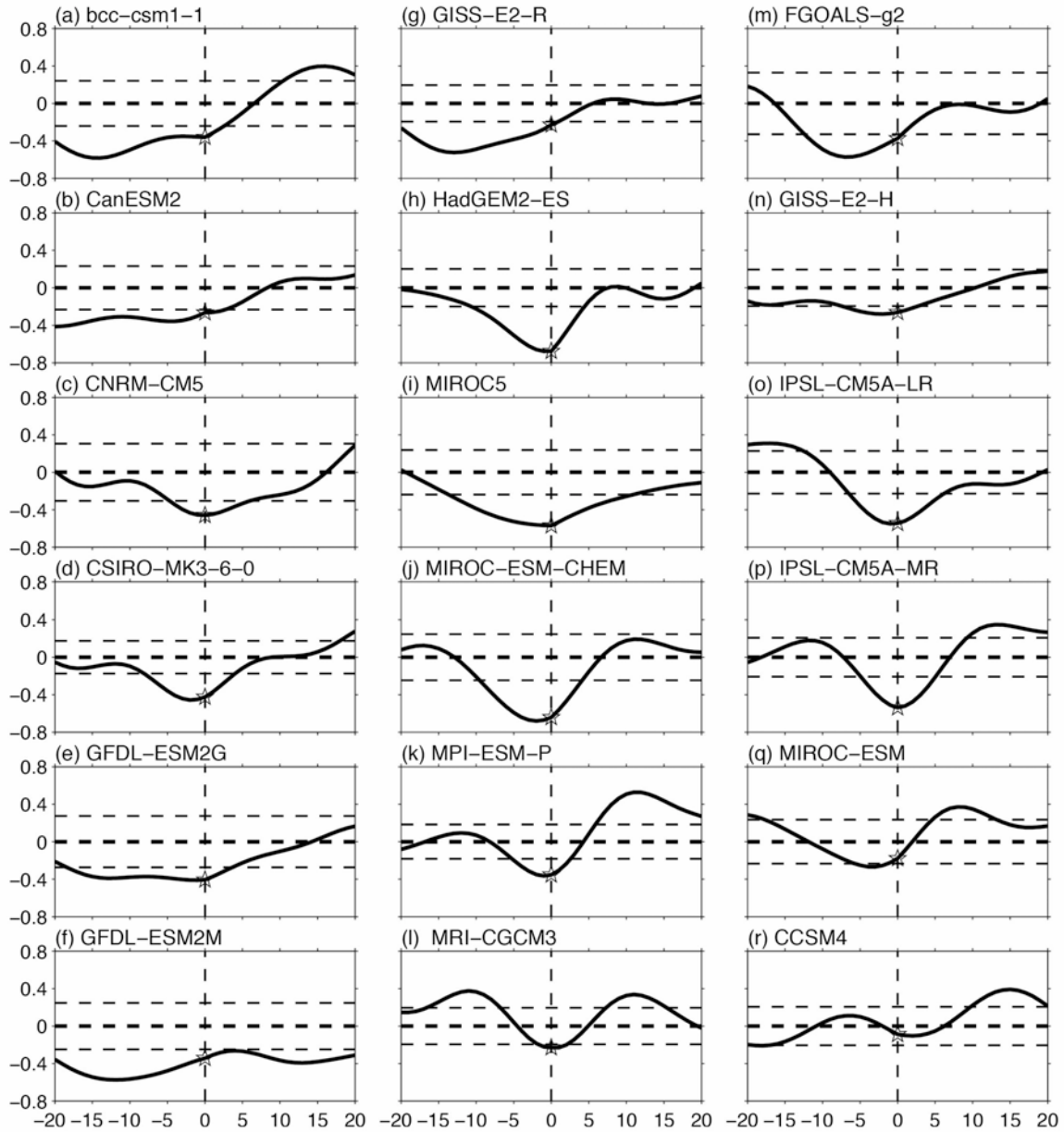
1



2
3
4
5
6

Figure 14. The Atlantic STC index defined as the maximum streamfunction in the upper 250 m between 5°N to 20°N from CMIP5 models. All time series are normalized by their standard deviation.

1

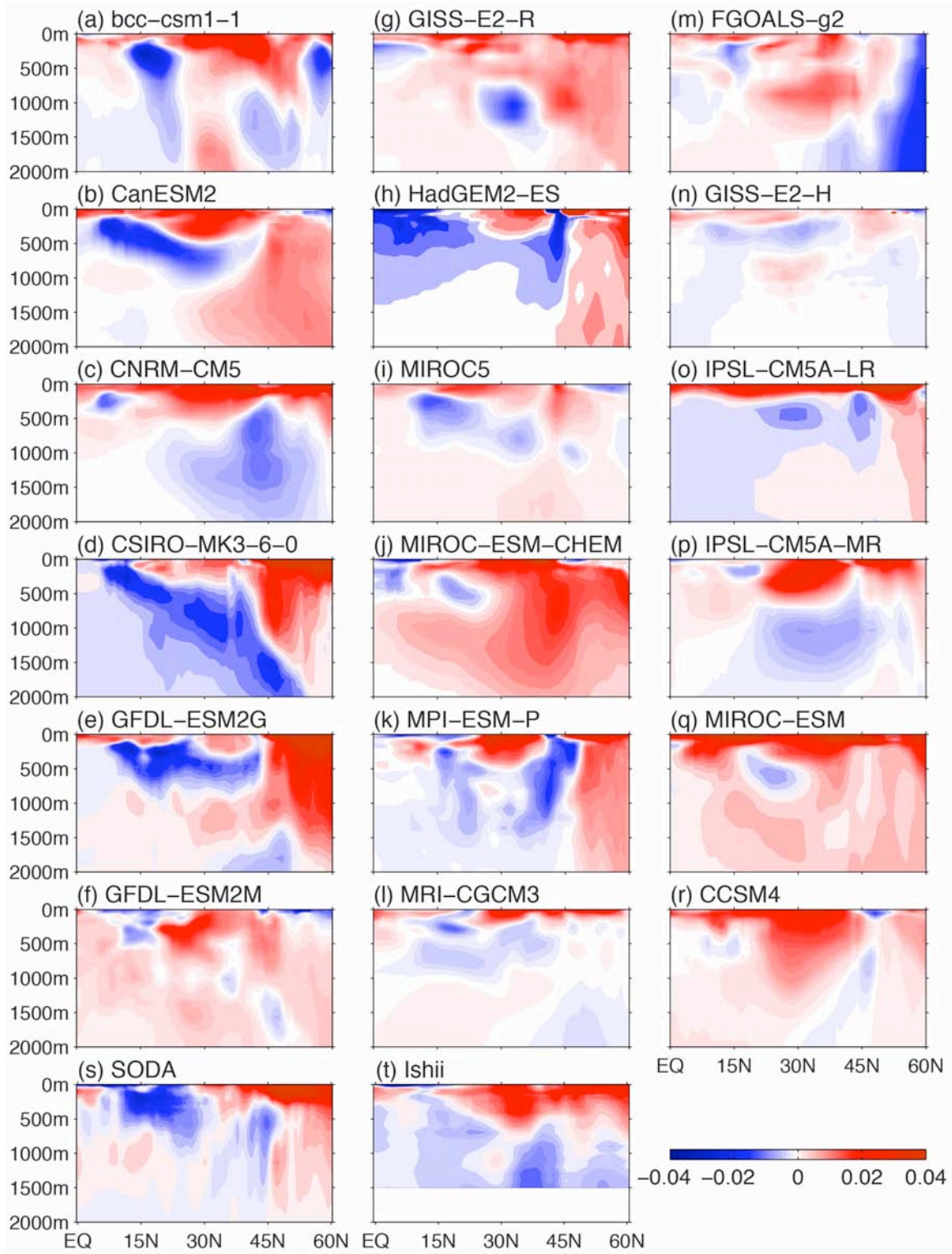


2

3

4 **Figure 15.** Lead-lag correlations between the AMO and STC index from CMIP5 models. The unit in x-axis is
5 year. Positive (negative) year in x-axis means the STC leads (lags) the AMO. The horizontal dash line indicates
6 the 90% confidence level.

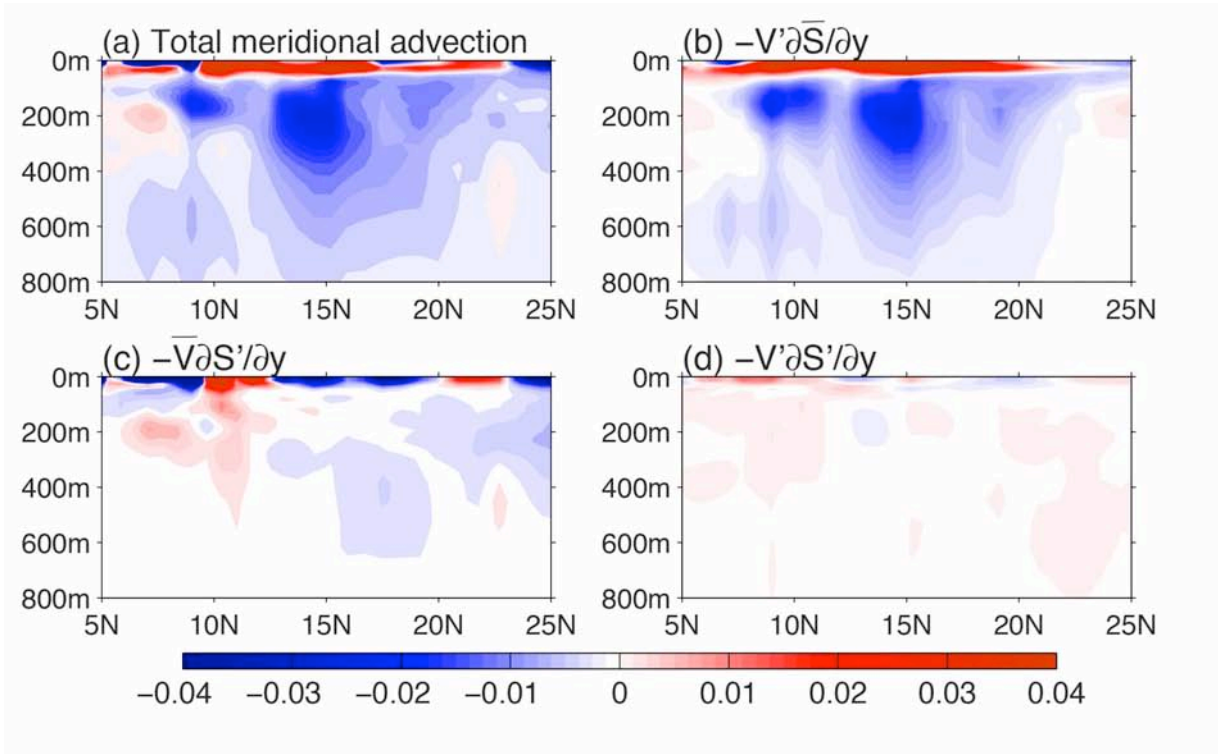
7



1
2
3
4
5

Figure 16. Regression of the Atlantic zonal mean salinity (psu) onto the normalized AMO index from (a-r) CMIP5 models, (s) SODA data and (t) Ishii data.

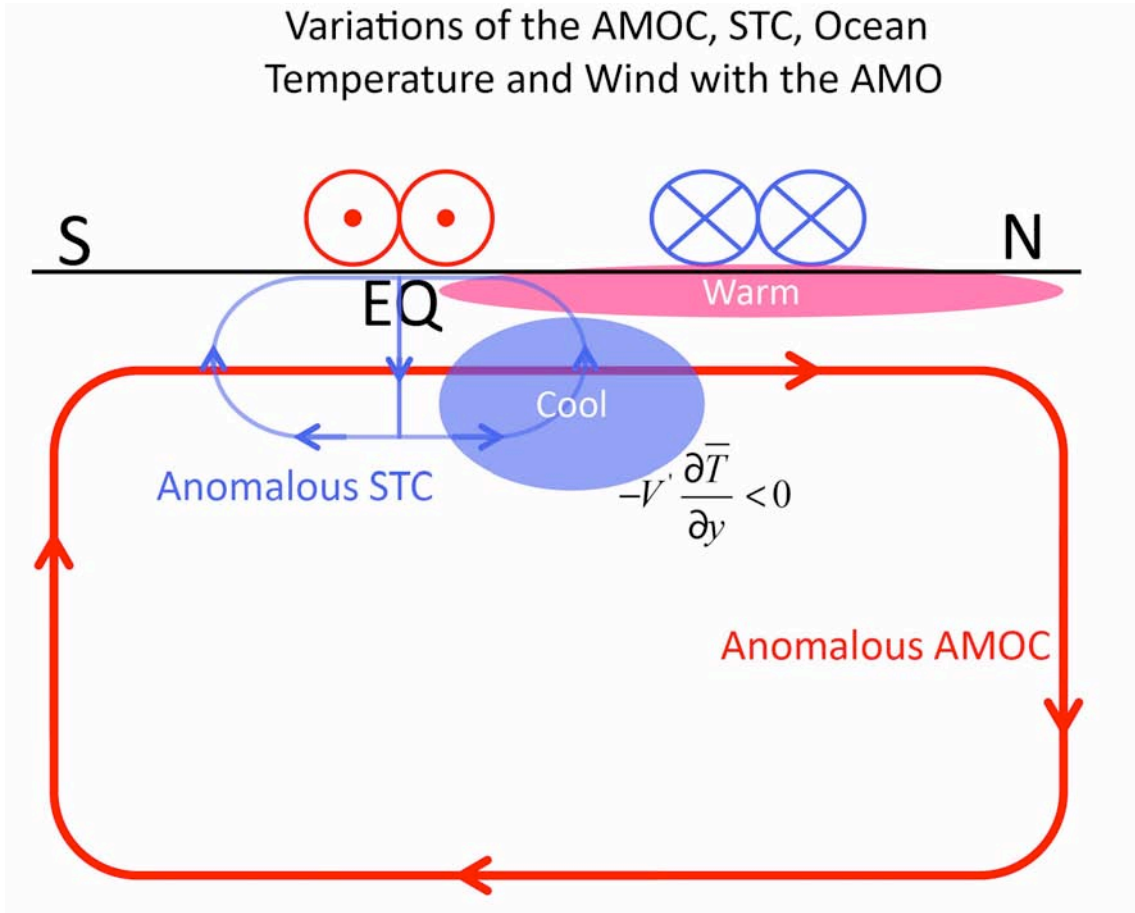
1
2
3



4
5
6
7
8
9
10

Figure 17. Regression of salinity advection terms (10^{-8} psu/s) onto the normalized AMO index. The regression is the ensemble mean of 12 CMIP5 models that simulate the TNA surface and subsurface temperature variation reasonably well. Shown are the (a) total meridional salinity advection, (b) advection by the anomalous meridional current, (c) advection by the mean meridional current, and (d) nonlinear term.

1
2
3



4
5
6
7
8

Figure 18. Schematic diagram showing the variations of the AMOC, STC, ocean temperature and surface wind with the AMO on multidecadal timescales.